High Field Electric Conduction in Polyimide

By

Nian-Rong Tu

A Thesis
Submitted to the Faculty of Graduate Studies
in Partial Fulfillment of the Requirements
for the Degree of
Master of Science

Department of Electrical and Computer Engineering
University of Manitoba
Winnipeg, Manitoba, Canada

ISBN 0-612-13538-1

Canada

Name Applied Sciences

Dissertation Abstracts International is arranged by broad, general subject categories. Please select the one subject which most nearly describes the content of your dissertation. Enter the corresponding four-digit code in the spaces provided.

Electronics and Electrical

SUBJECT TERM

0544

SUBJECT CODE

U·M·I

Subject Categories

THE HUMANITIES AND SOCIAL SCIENCES

COMMUNICATIONS AND THE ARTS

- Architecture 0729
- Art History 0377
- Cinema 0900
- Dance 0378
- Fine Arts 0357
- Information Science 0723
- Journalism 0391
- Library Science 0399
- Mass Communications 0708
- Music 0413
- Speech Communication 0459
- Theater 0465

EDUCATION

- General 0515
- Administration 0514
- Adult and Continuing 0516
- Agricultural 0517
- Art 0273
- Bilingual and Multicultural 0282
- Business 0688
- Community College 0275
- Curriculum and Instruction 0727
- Early Childhood 0518
- Elementary 0524
- Finance 0277
- Guidance and Counseling 0519
- Health 0680
- Higher 0745
- History of 0520
- Home Economics 0278
- Industrial 0521
- Language and Literature 0279
- Mathematics 0280
- Music 0522
- Philosophy of 0998
- Physical 0523
- Psychology 0525
- Reading 0535
- Religious 0527
- Sciences 0714
- Secondary 0533
- Social Sciences 0534
- Sociology of 0340
- Special 0529
- Teacher Training 0530
- Technology 0710
- Tests and Measurements 0288
- Vocational 0747

LANGUAGE, LITERATURE AND LINGUISTICS

- Language
  - General 0679
  - Ancient 0289
  - Linguistics 0290
  - Modern 0291
- Literature
  - General 0401
  - Classical 0294
  - Comparative 0295
  - Medieval 0297
  - Modern 0298
  - African 0316
  - American 0591
  - Asian 0305
  - Canadian (English) 0352
  - Canadian (French) 0355
  - English 0593
  - Germanic 0311
  - Latin American 0312
  - Middle Eastern 0315
  - Romance 0313
  - Slavic and East European 0314

PHILOSOPHY, RELIGION AND THEOLOGY

- Philosophy 0422
- Religion
  - General 0318
  - Biblical Studies 0321
  - Clergy 0319
  - History of 0320
  - Philosophy of 0322
- Theology 0469

SOCIAL SCIENCES

- American Studies 0323
- Anthropology
  - Archaeology 0324
  - Cultural 0326
  - Physical 0327
- Business Administration
  - General 0310
  - Accounting 0272
  - Banking 0770
  - Management 0454
  - Marketing 0338
- Canadian Studies 0385
- Economics
  - General 0501
  - Agricultural 0503
  - Commerce-Business 0505
  - Finance 0508
  - History 0509
  - Labor 0510
  - Theory 0511
- Folklore 0358
- Geography 0366
- Gerontology 0351
- History
  - General 0578
  - Ancient 0579
  - Medieval 0581
  - Modern 0582
  - Black 0328
  - African 0331
  - Asia, Australia and Oceania 0332
  - Canadian 0334
  - European 0335
  - Latin American 0336
  - Middle Eastern 0333
  - United States 0337
- History of Science 0585
- Law 0398
- Political Science
  - General 0615
  - International Law and Relations 0616
  - Public Administration 0617
- Recreation 0814
- Social Work 0452
- Sociology
  - General 0626
  - Criminology and Penology 0627
  - Demography 0938
  - Ethnic and Racial Studies 0631
  - Individual and Family Studies 0628
  - Industrial and Labor Relations 0629
  - Public and Social Welfare 0630
  - Social Structure and Development 0700
  - Theory and Methods 0344
- Transportation 0709
- Urban and Regional Planning 0999
- Women's Studies 0453

THE SCIENCES AND ENGINEERING

BIOLOGICAL SCIENCES

- Agriculture
  - General 0473
  - Agronomy 0285
  - Animal Culture and Nutrition 0475
  - Animal Pathology 0476
  - Food Science and Technology 0359
  - Forestry and Wildlife 0478
  - Plant Culture 0479
  - Plant Pathology 0480
  - Plant Physiology 0817
  - Range Management 0777
  - Wood Technology 0746
- Biology
  - General 0306
  - Anatomy 0287
  - Biostatistics 0308
  - Botany 0309
  - Cell 0379
  - Ecology 0329
  - Entomology 0353
  - Genetics 0369
  - Limnology 0793
  - Microbiology 0410
  - Molecular 0307
  - Neuroscience 0317
  - Oceanography 0416
  - Physiology 0433
  - Radiation 0821
  - Veterinary Science 0778
  - Zoology 0472
- Biophysics
  - General 0786
  - Medical 0760

EARTH SCIENCES

- Biogeochemistry 0425
- Geochemistry 0996
- Geodesy 0370
- Geology 0372
- Geophysics 0373
- Hydrology 0388
- Mineralogy 0411
- Paleobotany 0345
- Paleoecology 0426
- Paleontology 0418
- Paleozoology 0985
- Palynology 0427
- Physical Geography 0368
- Physical Oceanography 0415

HEALTH AND ENVIRONMENTAL SCIENCES

- Environmental Sciences 0768
- Health Sciences
  - General 0566
  - Audiology 0300
  - Chemotherapy 0992
  - Dentistry 0567
  - Education 0350
  - Hospital Management 0769
  - Human Development 0758
  - Immunology 0982
  - Medicine and Surgery 0564
  - Mental Health 0347
  - Nursing 0569
  - Nutrition 0570
  - Obstetrics and Gynecology 0380
  - Occupational Health and Therapy 0354
  - Ophthalmology 0381
  - Pathology 0571
  - Pharmacology 0419
  - Pharmacy 0572
  - Physical Therapy 0382
  - Public Health 0573
  - Radiology 0574
  - Recreation 0575
  - Speech Pathology 0460
  - Toxicology 0383
- Home Economics 0386

PHYSICAL SCIENCES

Pure Sciences

- Chemistry
  - General 0485
  - Agricultural 0749
  - Analytical 0486
  - Biochemistry 0487
  - Inorganic 0488
  - Nuclear 0738
  - Organic 0490
  - Pharmaceutical 0491
  - Physical 0494
  - Polymer 0495
  - Radiation 0754
- Mathematics 0405
- Physics
  - General 0605
  - Acoustics 0986
  - Astronomy and Astrophysics 0606
  - Atmospheric Science 0608
  - Atomic 0748
  - Electronics and Electricity 0607
  - Elementary Particles and High Energy 0798
  - Fluid and Plasma 0759
  - Molecular 0609
  - Nuclear 0610
  - Optics 0752
  - Radiation 0756
  - Solid State 0611
- Statistics 0463

Applied Sciences

- Applied Mechanics 0346
- Computer Science 0984
- Engineering
  - General 0537
  - Aerospace 0538
  - Agricultural 0539
  - Automotive 0540
  - Biomedical 0541
  - Chemical 0542
  - Civil 0543
  - Electronics and Electrical 0544
  - Heat and Thermodynamics 0348
  - Hydraulic 0545
  - Industrial 0546
  - Marine 0547
  - Materials Science 0794
  - Mechanical 0548
  - Metallurgy 0743
  - Mining 0551
  - Nuclear 0552
  - Packaging 0549
  - Petroleum 0765
  - Sanitary and Municipal 0554
  - System Science 0790
- Geotechnology 0428
- Operations Research 0796
- Plastics Technology 0795
- Textile Technology 0994

PSYCHOLOGY

- General 0621
- Behavioral 0384
- Clinical 0622
- Developmental 0620
- Experimental 0623
- Industrial 0624
- Personality 0625
- Physiological 0989
- Psychobiology 0349
- Psychometrics 0632
- Social 0451

HIGH-FIELD ELECTRIC CONDUCTION IN POLYIMIDE

BY

NIAN-RONG TU

A Thesis submitted to the Faculty of Graduate Studies of the University of Manitoba in partial fulfillment of the requirements of the degree of

MASTER OF SCIENCE

I hereby declare that I am the sole author of this thesis.

I authorize the University of Manitoba to lend this thesis other institutions or individuals for the purpose of scholarly research.

Nian-Rong Tu

I further authorize the University of Manitoba to reproduce this thesis by photocopying or by other means, in total or in part, at the request of other institutions or individuals for the purpose of scholarly research.

Nian-Rong Tu

Abstract

Electric conduction current in polyimide has been measured at high fields using metal(Au)-polyimide(P)-*p*-silicon(S)---MPS structure. On the basis of the current-voltage (I-V) characteristics coupled with the capacitance-voltage (C-V) characteristics measured under various conditions, it is found that electric conduction at high fields (>1.4 MV/cm) is mainly due to Fowler-Nordheim (FN) type tunneling injection of electrons from the Au gate electrode if it is negatively biased, or from the PI/Si contact if the Au gate electrode is positively biased. The conduction current is strongly dependent on the concentration and centroid location of the traps. Computer simulation reveals that the trap concentration is of the order of 10^{13} cm^{-2} with its centroid located near the electron injecting contact and that the trap ledge occurs only when the net negatively trapped electron charge is large and its centroid close to the injecting contact. If the centroid is not close to the injecting contact, the trap concentration must be large in order to create an internal field with the rate of increase equal to the ramp rate of the applied field.

The decay of the dark charging current under a dc field, is associated mainly with the time dependent trap-filling process, while the decay of the dark discharging current is associated mainly with the time dependent detrapping process. The photoconduction under an ultra violet (UV) light illumination is due mainly to the photogenerated free holes. Electric conduction and breakdown strength are strongly dependent on the humidity of the environment in which they are exposed.

Acknowledgments

The author would like to thank his advisor, Prof. K. C. Kao, for his generous support and intellectual guidance throughout the years of graduate studies. His insightful advice, clear vision, many suggestions, endless efforts and many educational discussions are invaluable. The author would also like to thank Prof. D. J. Thomson for his helpful and cordial advice. The author is also indebted to his colleagues and fellow students of the Materials and Devices Research Laboratory for their stimulating discussion and technical assistance, particularly T. T. Chau and L. Kan. Special thanks is given to Deane Lam for her encouragement.

Finally, the financial support from National Sciences and Engineering Research Council of Canada (NSERC) for this research is gratefully acknowledged.

Contents

List of Figures

Chapter 1

Introduction

As the present trend for microelectronics is to make devices and other components smaller in size, faster in response, and more powerful in output, the demand on both the material and the fabrication processing becomes more crucial. The microelectronics industry has so far used exclusively inorganic materials such as silicon dioxide and silicon nitride, for insulation and passivation in integrated circuits or hybrid devices. There have been mounting concerns about these inorganic materials because they may not be able to meet the requirement for future VLSI or ULSI designs, especially in terms of planarization, surface cracking, dielectric behavior, mechanical stress, thermal stability, and reliability. To search for suitable materials with a better performance in insulation and passivation, there is a growing interest in the use of organic polymers to either supplement or replace inorganic materials.

Polyimide has become one of the most important polymers having the potential for microelectronics applications because of its good electric properties, high temperature stability, relatively good planarization, and easy processing[1,2]. A great deal of work, both experimental and theoretical, has been reported in the past two decades about this material[3-8]. If polyimide is used as a dielectric layer for MOS devices or multiple level metallization structure, the electric conduction at high fields is of importance because it may affect the long term reliability of the system. For polyimide, most work on electric conduction is limited to low fields(<500 kV/cm). Electric conduction at high fields (>500 kV/cm) has rarely been reported. Up to present, the question about the dominant carrier species responsible for electric conduction at high fields and final breakdown in polyimide are still in dispute. An experimental method to determine the dominant carrier species at very high fields can be considered as the first step to study the high field dielectric behavior in polymers. This is the objective of this research to carry out a series of experiments in order to determine the type of carrier species at high fields. To do this, we adopted the techniques already commonly used for studies of thin silicon dioxide films. These techniques involve the measurements of current-voltage (I-V) characteristics using linearly ramp voltage of various ramp rates, and also the measurements of corresponding high frequency capacitance-voltage (C-V) characteristics. The advantage of using these techniques coupled with thin film samples are that very high field can be easily obtained at a relatively low applied voltage.

In this thesis a brief review is given in chapter 2 on the recent development in synthesis, properties and applications of polyimide. Chapter 3 presents the techniques, experimental results on electric conduction at high fields, and discussion. Some results about the effects of humid environment on the electric conduction and breakdown are also included in this chapter because polyimide is quite permissible to moisture. It is well known that moisture absorption usually lend to degradation of chemical and electrical properties of the material.

In order to study further the effects of bulk traps in polyimide, we have also carried out a preliminary study on photoconduction. Photoconduction provide another probe to study the carrier transport in polyimides. In insulating polymers, it is well known that there is always a longtime decay of the charging current after the application of a dc field and the discharging current after the removal of the applied field and short-circuiting of the two electrodes. The charging current may be due to the trap-filling process while the discharging current due to the detrapping process. If the photoconduction current is measured during the charging and discharging periods, the photocurrent transient may reveal the carrier species responsible for photoconduction. The details of the phototransient phenomenon are discussed in chapter 4. The final conclusions based on all the experimental work are given in chapter 5.

Chapter 2

Brief Review on Synthesis, Properties, and Applications of Polyimides

Polyimde (PI) films are widely used in electronics industry as an interlayer dielectric and passivation materials as well as for other applications. PI films provide excellent step coverage and can be coated to form very thin layers. In this chapter, synthesis, properties and applications of polyimide will be briefly reviewed.

2.1 Synthesis of Polyimide

Polyimide were developed during the 1960's and early 1970's in response to the demands of the aerospace industry for polymers having good high temperature performance, as matrix materials for laminates and other composites. Most aromatic/ heterocyclic polymer systems that have a small number of oxidizable C-H bonds per molecule exhibit excellent oxidative stability, but tend to be intractable and extremely difficult to process. In the case of polyimide, however, this limitation has been largely overcome. Some of the materials now in use for structure applications can withstand continuous exposure in air to temperature above 500^0 C.

The characteristic structure feature of polyimide is the presence of the phthalimide grouping in the repeat unit, which is represented by the formula,

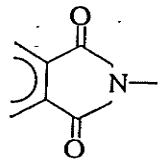

These units may be linked through alkyl or aryl groups to form the main polymer chain, the latter generally giving good higher temperature performance.

The most general method for preparation of high temperature polyimide is based on the reaction between an aromatic diamine and an aromatic dianhydride or carboxylic acid [9]. This proceeds via the formation of the intermediate polyamic acid which in further heating undergoes a ring closure condensation reaction leading to imide formation. This reaction is as follows,

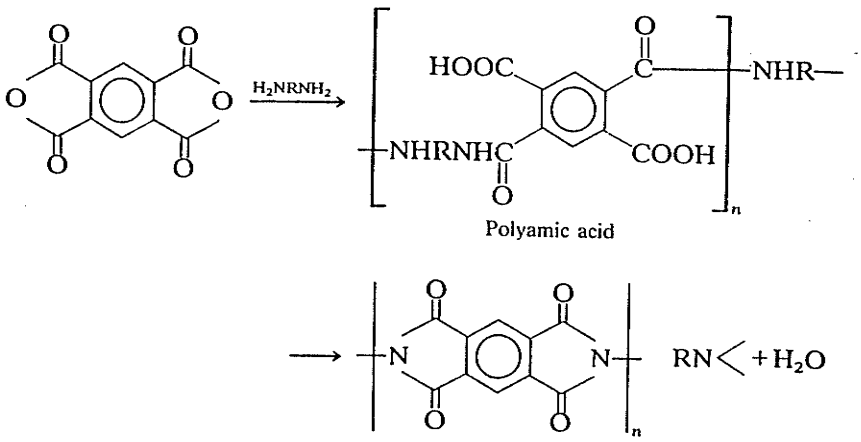

The fact that water is eliminated during the final cure to produce a highly condensed polymer with rapidly increasing viscosity (low flow) results in a relatively high

concentration of voids, removal of which requires heating above T_g (typically > 200°C) for longer than 30 minutes.

In the late 1960's, another class of polyimides was developed in which the anhydride or acid is replaced by a bismaleimide and the resulting polyimide is formed without elimination of water. The reaction illustrated schematically below proceeds via amine addition about the double bonds of bismaleimide to form a linear prepolymer. In the presence of excess bismaleimide and a free radical initiator, self addition can occur at the maleic double bond leading to crosslinking which produces a polymer of high thermal stability.

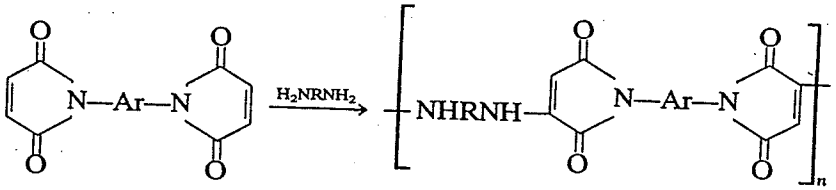

2.2 Curing behavior of polyimide

The curing behavior of the polyimides is often an important consideration, especially in situations where etching is performed at intermediate cure levels. Imidization (ring formation) of polyamic acids is an important process characteristic for determining mechanical and thermochemical properties. Infrared absorption spectroscopy is a useful technique for determining the level of imidization of polyimide. Kreutz *et al*[10] used 725 cm^{-1} imide absorption to study the cyclization reaction of polyamic acids films derived from pyromellitic dianhydride and 4, 4'-diaminodiphenyl ether. They observed that the ring closure reaction proceed as a two

step processes, characterized by an initial rapid cyclization reaction which changed into a substantially slower cyclization process. The change in rate was attributed to either the increase in chain stiffness as the cyclization proceeded or to the loss of the solvent. The acceleration of the imidization process by the presence of solvent was also observed by Dine-Hart[11]. Ginsburg and Susko attributed the dependence of the degree of cure of PMDA/ODA on film thickness to increased solvent retention in the thicker films [12]. The two step behavior of the imidization process has been observed by several authors and it has been suggested that this behavior is related to the point at which the glass transition temperature is reached, that is, as the reaction proceeds, the glass transition temperature of the polymer increases. Denisov *et al* used IR spectroscopy to monitor the imidization process, using either the intensification of the imide ring bands at 1780 cm^{-1}, 1330 cm^{-1}, and 730 cm^{-1}, or on the basis of the reduced intensity of the bands for the NH group in the 3280 cm^{-1}, and 1540 cm^{-1} regions [13]. Krasovskii *et al* [14] explored methods of qualifying the degree of imidization at high degrees of imidization, and found that the strong amide (1660 cm^{-1}) vibration could be used if a curve deconvolution was employed in this spectral region where three bands (the benzene ring mode at 1600cm^{-1} and the imide I mode at 1720 cm^{-1}) overlap. For example, a typical IR spectrum of PI is shown in figure 2.1 for the cure temperature at 135°C and 350 °C [15].

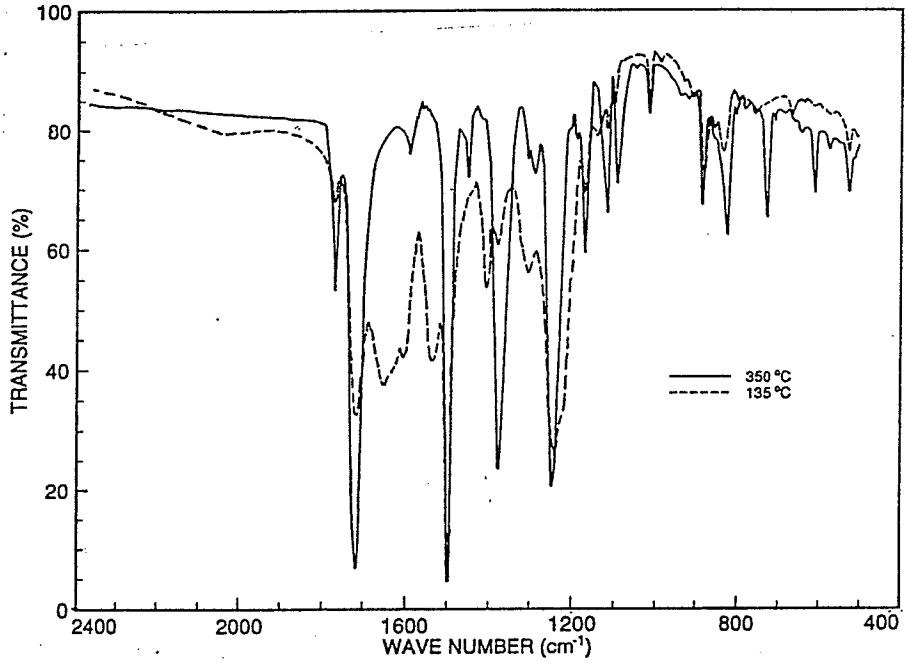

Figure 2.1: *IR spectrum of polyimide cured at different temperature (After Kan and Kao, [15])*

Morphology changes that occur during a thermal cure has also been monitored through fluorescence spectroscopy to study the change of two kinds of polyimides, PMDA-ODA and BTDA-ODA. To account for the fact that excitation ofeither the low or the long wavelength bands, assigned to the π-π^* and n-π^* transitions of the aromatic substituted pyromellitimide moiety, respectively, in either PMDA-ODA or BTDA-ODA results in a similar emission spectrum each, it is proposed that a charge transfer complex (CTC) is formed between the diamine (donor) and divide (acceptor). More specifically, the increase in fluorescence

intensity, arising from π-π^* excitation, with increasing cure temperature is attributed to a conformational change whereby the number of adjacent moities that are able to form intramolecular CTC's via π-conjugation is increased. For n-π^* excitation, these thermally induced intensity changes are accounted for by increased intermolecular CTC formation with decreased interchain distance. Although the degree of aggregation increases with cure, the specific morphology changes are still a subject of controversy [16-19]. The magnitude of interchain distance (4.7 to 5.7 Å) requires that the aromatic rings associated with the dianse moiety to be coplanar. Moreover, it is reported that in the crystalline phase, the morphology is such that adjacent chains are aligned such like moities face each other [20]. Morphology affects the refractive index (RI) and this effects must be considered in the future applications utilizing polymers in optical signal processing. Uniaxial deformation of polyamic acid films results in significant orientation of the polymer chains along the stretching axis and it was enhanced during the thermal cure process. PMDA-PDA exhibits a greater molecular chain orientation relative to PMDA-ODA for similar elongation ratios and it was attributed to the rigid -rod nature of the PMDA-PDA chain.

2.3 The relationship between structures and properties

The properties of polyimide are strongly dependent on the chemical structure. For example, the polyimide prepared from 4, 4'-diaminodiphenyl ether, which has commercial applications use as a plastic or a coating, has a melting point in excess of

600° C and exhibits almost no weight loss at temperature up to 500° C under an inert atmosphere. Polyimide such as

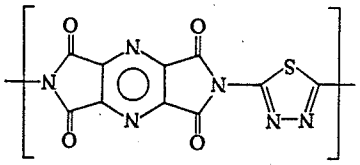

which contain no pendent hydrogen, have a greater thermal stability than the corresponding polyimide prepared from pyromellitic dianhydride (PMDA).

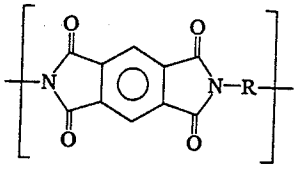

The chemistry and properties of polyimides containing carbonyl and ether connecting groups between the aromatic rings have been reported by Hergenrotler *et al.* They showed semi-crystalline polyimide, from the reaction between BTDA and 1,3-BBB, exhibited excellent resistance to strong base and high mechanical properties in the form of a film, adhesive and molding [21]. The crystallization rate was significantly enhanced by molecular weight control and end-capping without any substantial compromise in mechanical properties. Uniaxially stretched film exhibited more than twice the tensile strength and modules of unoriented film.

Recently, much work is under way to incorporate fluorinated segments in the polyimide macromolecules [22]. Hougham *et al* have reported incorporation of fluorinated segments had some interesting difference in their electrical and mechanical behavior [23]. The substitution of aromatic ring bond hydrogen with fluorine seems to effect moderate decreases in the dielectric constant, moderate

increases in the β transition allows a more stable dielectric responses as a function of temperature which can be important for the performance of electronic devices in hostile temperature environments. The thermal stability and coefficient of thermal expansion of these materials has not been appreciably effected by the substitution of fluorine for hydrogen.

Plasma treatment has been regarded a promising method to improve moisture resistance [24]. It has been found that the surface of the polyimide could be fluorinated by plasmas of CF_4 and oxygen. It has also been found that at the harsh plasma conditions used for etching, the fluorine did not only remain at the surface of the polymer, but diffuses into the bulk of the film as well. It has been reported that fluorine was introduced into the surface of the PI by exposure to NF_3 plasmas and fluorination was monitored with X-ray photoelectron spectroscopy and Fourier transform infrared absorption spectroscopy. Spectroscopic studies show that the aromatic carbons in the polymers are more readily fluorinated than carbonyl group carbons. The PI film surface are quickly fluorinated during plasma exposure, and the moisture resistance improves consequently by examining the water contact angle.

2.4. Properties of Polyimide Films

2.4.1 Electrical Properties

It has been found that dissipation factor D is related to the curing temperature[25]. D decreases with the increases of the curing temperature and curing time at temperature lower than 300°C due to solvent (H_2O) release and imidization.

After full imidization at temperature between 350 °C and 450 °C, the dissipation factor can reach 0.003 for Dupont PI 2545. The dissipation factor would increase if temperature is further increased due to decomposition of material. The dielectric constant is 3.2 at 1 MHz as compared to 3.9 for thermally grown SiO_2. The lower dielectric constant is an advantage over SiO_2 since it reduces capacitance and hence the propagation time in integrate circuits.

The level of electrical conductivity of polyimide films is obviously of great importance in their potential application to the integrated circuit fabrication. The electrical properties of PI2545, PI2555 and Hitachi PIQ are all consistent with good interlevel dielectric performance. At a typical field of $5x10^5$ V/cm, the conductivity is $\sim 10^{-16}$ ohm $^{-1}$ cm^{-1} which is similar to that of thermally grown SiO_2. At higher fields such as $2x10^6$ V/cm, the conductivity of polyimide increases several orders of magnitude over the thermal SiO_2 (to $\sim 3x10^{-13}$ ohm $^{-1}$ cm^{-1})[26].

Electric conduction in polyimide has received considerable attention[27-34]. Nevin *et al* [28] have reported that the conduction mechanism in polyimide at low temperature (<100 ° C) and low electric fields has been identified as due to a combination of the Schottky emission and Frenkel-Poole detrapping process. However, for a long time and at a high temperature (>100 °C), the transport current tends to dominate. The transport current is ohmic and is found to be temperature dependent.

On the other hand, Neuhaus *et al* studied the transient currents in pure and Na^+ -doped PI films with Al and Au electrodes [35]. They reported that electric

conduction is not ionic but is an electronic transport process. The electronic conduction is modulated by the presence of mobile ionic impurities, the current and total charge transport vary in proportion to the Na ions in the film. They also found that transient current in PI is initially dominated by the ionic redistribution.

For the dielectric strength of PI, Hikita *et al* have reported that polyimide electric strength of polyimide has a negative temperature dependence, and a positive voltage rise rate dependence, and the current has a functional form of thermally activated type conduction [36]. Prebreakdown current increases rapidly within a period of about 1 ms before breakdown indicating that breakdown is associated with thermal instability.

2.4.2 Photoconduction in Polyimides

The photoconductivity of polyimide film has been studied using UV, X-ray and visible radiation as the radiation source[15,37]. The photoconduction in polyimide was first reported by Takai *et al* [37]. They have reported that two photocurrent peaks at 2.70 eV and 3.65 eV are independent of electrode materials and applied voltage polarities. X-ray diffraction indicates that the photocurrent of polyimide is influenced by the molecular order. The photocurrent increases with the reduction in molecular ordering and it is due to the increase in the photogeneration efficiency. Unlike the photoconduction in the visible region, in the ultraviolet region, it has been observed that the dependence of both the material and the applied voltage polarity of the illuminated electrode in polyimide. Kan and Kao found four

absorption peaks located at 3.65, 4.35, 5.65, and 6.40 eV in the fully cured polyimide films [15]. The peak at 6.40 eV is practically independent of the curing temperature, but the other three peaks increases with increasing curing temperature. In the photo quantum efficiency spectra, there are also four peaks in the fully cured polyimide films but they are located at 3.55, 4.05, 4.90, and 5.80 eV. The quantum efficiency increases with increasing applied field, following closely the Onsage theory.

Although polyimides are well known for its good insulating characteristics, the low quantum yield of the photogeneration has limited the utility of these materials as photoconductors. Freilich has reported that the addition of electron donors to Kapton polyimide film results in an enhancement of photocurrent as much as 5 orders of magnitude in the range of 105 to 106 v/cm as compared to the virgin polymer without significantly sacrifice other positive feature of polyimide [7]. The mechanism of the enhancement is the result of radiation absorption by the charge-transfer complex formed between the added electron donor and the imide portion of the polymer backbone. Excitation is followed by rapid and complete electron transfer from the donor to pyromellitimide to yield the radical anion of the polymer and the radical cation of the donor. Figure 2.2 shows photoresponse as a function of the applied field for pure Kapton polyimide and 0.3 mil DMA/Kapton.

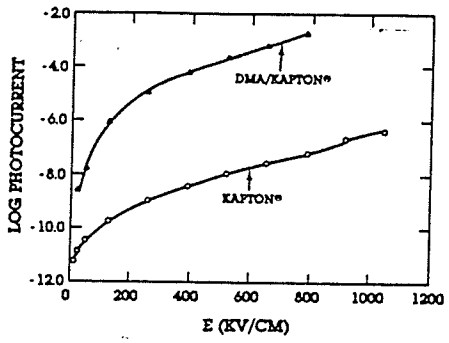

Figure 2.2: *Photocurrent response (A/cm^2) as a function of applied field for 0.3-mil Kapton and 0.3-mil DMA/Kapton. Illumination is carried out at 480 nm(after Freilich, [7]).*

2.4.3 Moisture Effects on the Performance of Polyimide Films

Although polyimide has several advantages that make it attractive for microelectronics applications, there are potential problems associated with PI usage. The foremost of these is that PI absorbs moisture. Moisture can lead to such reliability problems in integrated circuits as increase of insulator conductivity, loss of adhesion, and corrosion[38,39]. The moisture uptake in PI is found to be linearly related to ambient relative humidity, and the maximum moisture uptake by weight is 3.2%. The permitivity of PI films near room temperature increases up to 20% due to the absorption of the water. By their investigation, the moisture uptake is a bulk absorption rather than a surface adsorption phenomenon. Xu *et al* use dielectric loss measurements and NMR spectroscopy to investigate the effects of water on the dielectric properties of Kapton and spin-on PMDA-ODA films [40]. They conclude that there are two different kinds of sites in which water resides in PI. One of the sites

is associated with PI in the bulk of the film and the other site is associated with the PI near the surface. By investigating the complex permitivity of DuPont Kapton PI over the range from 80 K to 325 K, Melcher *et al* report the binding of the water molecules to different sites in neibouring PI chains as shown in figure 2.3 [41]

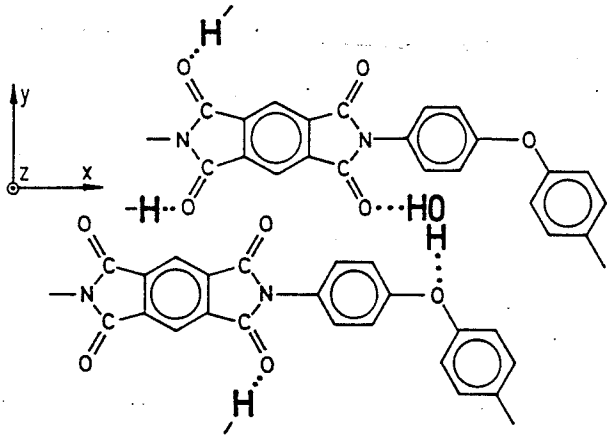

Figure 2.3: *Repeat units of a PI molecule. The possible sites for water molecule are indicated schematically(after Melcher, et al [41]).*

Water absorption also has large effect on the electric conduction in PI. Figure 2.4 shows the current density J against electric field F characteristics at 90 ° C for as received PI and PI which had undergone water absorption treatment for seven days reported by Hikita *et al* [36]. The current density of PI with water absorption is larger by one order of magnitude than that as received PI. The reason they give is that the water contained in the PI film decreases the dissociation energy of ions, which leads to an increase in the number of mobile ion.

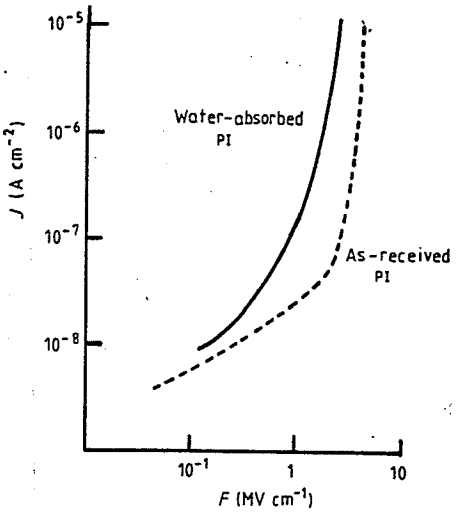

Figure 2.4: *Current density J against electric field F at 90^0 C for as-received PI and PI has undergone water absorption treatment for several days (after Hikita, et al [36])*

2.4.4 Interface and Adhesion of Polyimides

One of the most important concern of polyimide materials is to achieve good adhesion to semiconductor materials and metals. The adhesion of polyimide to Si and SiO_2 is good, but after prolonged exposure to electrical stressing, it tends to degrade. The Dupont VM651 adhesion promoter can improve the long term stability of PI-Si and PI-SiO_2 interface. For metals, aluminum has been used for a conventional wiring material of semiconductor devices. Polyimides have good adhesion to aluminum. However, in order to prevent the corrosion and migration of aluminum which decreases the reliability of semiconductor devices, copper or copper doped aluminum alloy has come to be used. It is well known that polyimide formed on copper deteriorates when heated at high temperature. Vchimura *et al* studied the

interface properties of copper and PI [42]. They found Cu to distribute normally along the direction of Cu/PI interface to polyimide surface and diffuse into PI film during PI curing stage. Gonsalres *et al* achieved the modification of copper layer through chemical and electrochemical modification with an ultrathin copper ferricyanide [43]. The modified surface was characterized by FTIR and x-ray powder diffraction. The effects on the adhesion of polyimide films onto the modified copper substrate were examined by the peel test. Enhanced adhesion between copper and polyimide was observed on the modified copper surface. The formation of the chemical bonds between the metal and polyimide may give rise to the observed improved adhesion.

2.5 Applications of Polyimide

2.5.1 Passivation Layer

The most popular use for polyimide is as a passivation layer. A passivation layer provides protection from moisture corrosion, ion transport, and damage during packaging. The presence of pinhole defects in a passivation layer for integrated circuits may be reduced or eliminated by the use of a polyimide topcoat over the commonly used passivation coating of phosphosilicate glass (PSG) or silicon nitride. The chance of defects from two separate coats occurring at the same position is highly unlikely. Therefore, the use of polyimide as a second protective coating leads to improved yield and enhanced reliability. Dielectric coatings such as oxides may induce a high level of phosphorous to lower the melting temperature for reflow. In

the presence of moisture, phosphorous forms phosphoric acid, which is corrosive to metal conductors. Although polyimide absorbs moisture, it provides an excellent moisture barrier[44]. Polyimide can act as an excellent sodium barrier. In addition, Polyimide offers an elongation property, providing superior mechanical protection from stress generated by compression during packaging. In general, devices coated with polyimide have lower leakage current and better reliability, and have shown superior protection from the damage due to scratching and compression compared to conventional pure SiO_2 passivation [45].

2.5.2 Alpha Particle Barrier

Alpha radiation emitted by trace amounts of naturally induced thorium and uranium isotopes in packaging materials is a source of nondestructive soft error problem in charge coupled devices(CCD) and dynamic memories. As the devices shrink geometrically and critical charge levels diminish, this problem becomes much more acute. Thus, the chance for a soft error to occur increases greatly from 16K to 64K RAM. Polyimide is free of radioactive trace produced in ceramics or other inorganic materials such as fillers in encapsulating materials. Alpha particle barrier is generally thicker than a standard passivation layer and can practically eliminate this problem.

2.5.3 Stress Buffer

Device failures related to mechanical stress during packaging are of a great concern, especially when the circuit density and die size increases. Bigger dies

result in more failures of plastic-encapsulated devices due to mechanical stress imposed on the die by the molding compound as well as failures due to metal line cracking. Conventional passivation materials such as silicon dioxide and silicon nitride can not absorb the stresses developed during the packaging. One approach to minimize the stress-related failures is to apply a compliant buffer layer that can absorb both the thermal and mechanical stresses developed during encapsulation. The buffer layer can be applied on either wafer layer or at the packaging level. At the packaging level, soft and tough polymers such as silicon die-coating materials are sometimes drop-dispensed on the die after wire bonding. These materials absorb the stresses caused by the mismatch in thermal expansion coefficient between the silicon wafer and the molding compound. However, these low module materials often creep during temperature cycling, resulting in wirebond breakage. On the other hand, photodefinable polyimide applied on the wafer level can be patterned directly to leave bond pads open, thus eliminating the problem of wirebond breakage.

2.5.4 Multilevel Structure

In fabricating mutilayer high density integrated circuits and packages, layer after layer of thin metal film is generally applied. Rapid changes in height over short distance can occur. These topographical irregularities impede successful layering. An interlayer insulation in such a structure must provide not only adequate insulation to isolation the electrical connection parts, but should also provide

sufficient planarizaton of the underlying to topography. Irregular surfaces may cause optical problems such as light reflection from the irregular surface.

As geometric size shrinks and circuit density increases, the traditional inorganic materials such as chemically vapor deposited (CVD) silicon dioxide, may no longer provide sufficient planarization. Polyimide is ideally suited for interlayer insulation applications because of its excellent planarization and electrical properties, high thermal stability, high purity, low defect density, easy in processing and etching, its temperature coefficient of expansion matching to that of aluminum. The multilevel interconnections containing polyimide layers have also been used in 64K DRAM fabrication since the early 1970's in IBM. The planarization control provided by polyimide minimizes notching and results in a more uniform metal thickness[46]. Figure 2.5 shows a two level metallization structure fabricated by the conventional SiO_2 method and the planarization method with PI. The conventional structure has many steps at metal layer edges and holes of insulating layers as shown in figure 2.5(a). Therefore, product of a three or more level structure is severally limited. However, PI insulation interlayer has an excellent metallization and more steps can be achieved. Photograph of five-level structure made by the PI technology is shown in figure 2.6.

2.5.5 Photosensitive Polyimide as Patterning Material

In microelectronics applications, the Polyimide must be patterned to provide interconnection pathways. This involves using organic photoresist or hard masks as etch templates for transferring the image from the photomask to the polyimide.

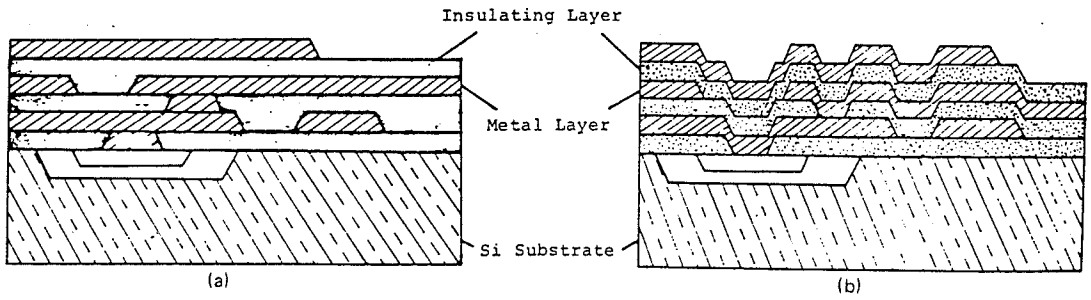

Figure 2.5: *Comparison of two-level metallization structure by (a) conventional structure and (b) PMP structure (after Sato, et al [47])*

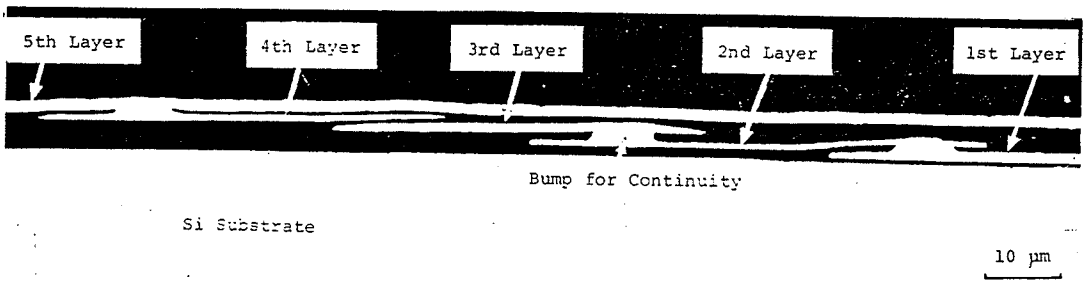

Figure 2.6: *Photograph of a five-level structure made by PMP technique(after Sato, et al [47])*

This indirect method is complicated by the processing steps required for applying, drying, patterning and stripping the photoresists or hard mask. In contrast, photosensitive polyimide can be patterned directly, without the need of photoresists or hard masks. Thermally stable polymeric precursors containing photoactive groups covalently bound to the polymer backbone have been developed[48]. Advancements in photodefinable polyimide systems have overcome a number of problems

associated with the first generation systems. It simplifies the manufacturing process by reducing the number of steps required for patterning polyimide coatings as shown in figure 2.7.

The basic component of photosensitive polyimide (PI2700) is a soluble polyimide precursor containing pendent photoreactive side groups as shown in figure 2.8. Upon exposure to ultraviolet radiation, the photoreactive groups undergo a free radical polymerization. This results in a solubility difference between the exposed and unexposed regions of the coating. The unexposed regions can be removed by dissolving them in a suitable solvent (developer). The remaining crosslinked intermediates are subsequently converted to a fully imidized polyimide by thermal cure. The resulting polyimide coating is the nearly the same as that produced from thermally imidizing the corresponding nonphotosensitive polyamic acid.

During the cure, the crosslinking bridges are volitilzed in the form of alcohols and polyalcohols. The volatilization of the crosslinking bridges results in a reduction in layer thickness without any significant loss in pattern resolution. The reduction in thickness occurs primarily in the vertical direction with little to no change in the lateral directions.

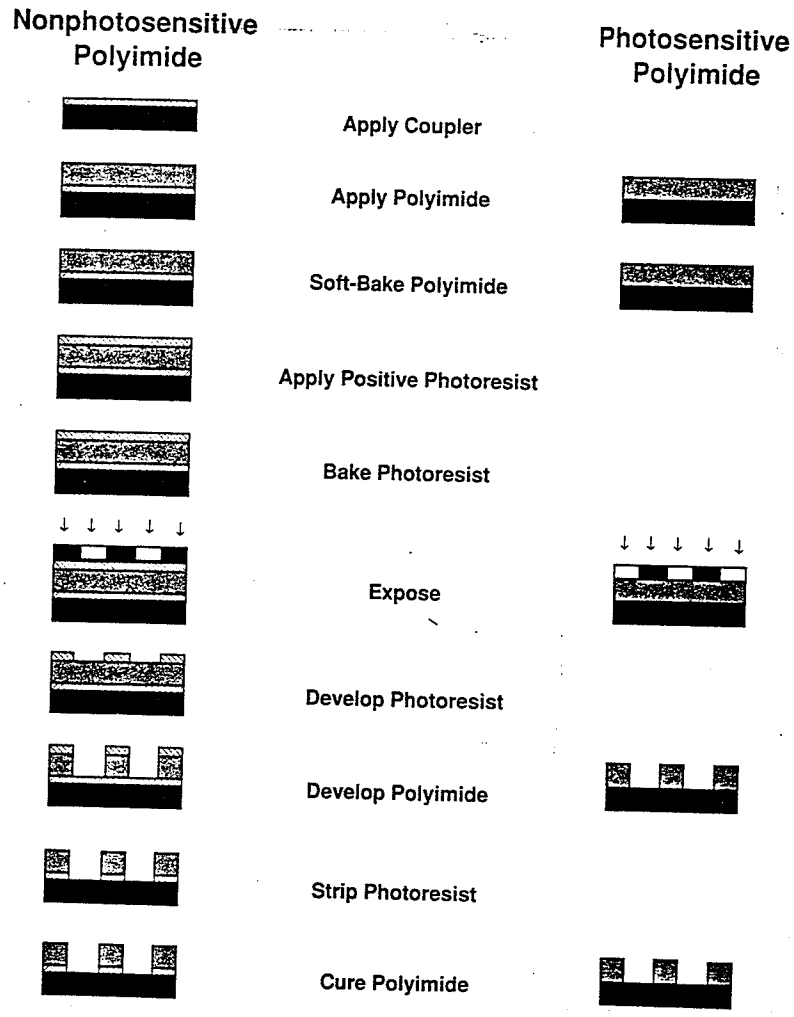

Figure 2.7: *Comparison of the number of processing steps required for a nonphotosensitive polyimide with those required for a photosensitive polyimide[49].*

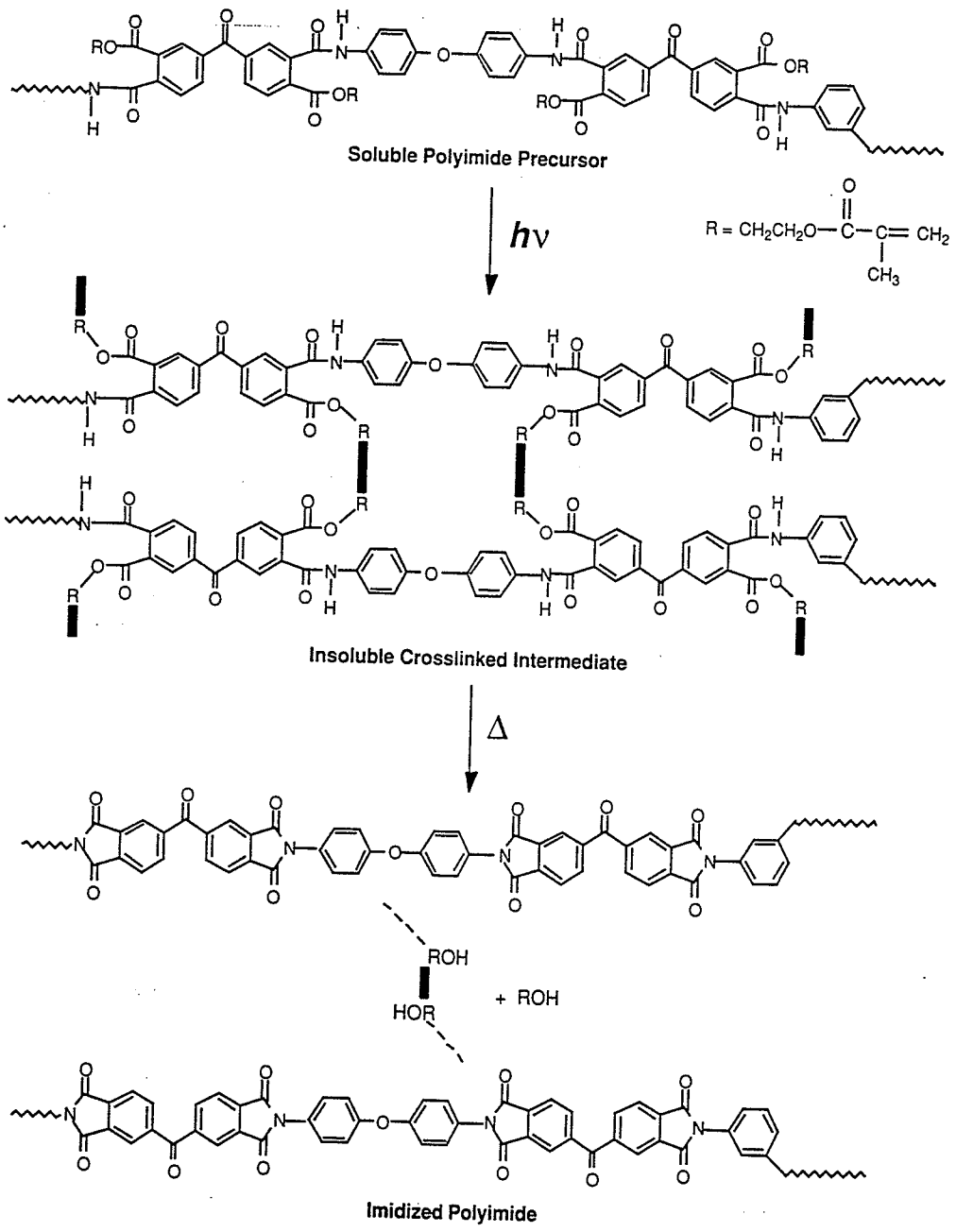

Figure 2.8: *Processing of a typical photosensitive polyimide showing general chemical reaction that occur at each step. (Structure shown for the PI 2701-2703 series from Dupont company[49])*

2.5.6 Humidity Sensor

The use of PI as moisture sensors has already been realized [50,51]. The mechanism of polyimide-based capacitive humidity sensor is based on the fact that the dielectric permitivity is nearly related to the ambient relative humidity. The equation for the dielectric constant is given by [50],

$$\varepsilon=[V_2(\varepsilon_2^{1/3}-\varepsilon_1^{1/3})+\varepsilon_1^{1/3}]^3$$

where ε_1 and ε_2 are the dielectric constants of the polymer and water respectively, and V_2 is the fractional volume of water absorbed. Because the absorption is a bulk phenomenon, the value of the maximum percent absorption will be independent of film thickness. Hence for thinner films, and thus larger capacitance, the absolute change in capacitance with relative humidity will be larger and thus easier to calibrate.

A typical sensor device is shown schematically in top view and cross section in Figure 2.9 . The upper electrode is 1-inch square and has 25 μm aluminum lines and 25 μm spaces to facilitate moisture diffusion into and out of the film. The capacitance measured at 1 kHz at room temperature and the capacitance increases by 35% from 0 to 100% RH. The transient behavior of the sensor has been investigated by exposing the capacitor to a step change in ambient RH- from 3 to 95%. The response time for dry to wet and wet to dry transitions is approximately 10 minutes. More rapid response can be achieved by using smaller finger width because a simple one dimension diffusion model predicts that the equilibrium time goes as the square of the finger width.

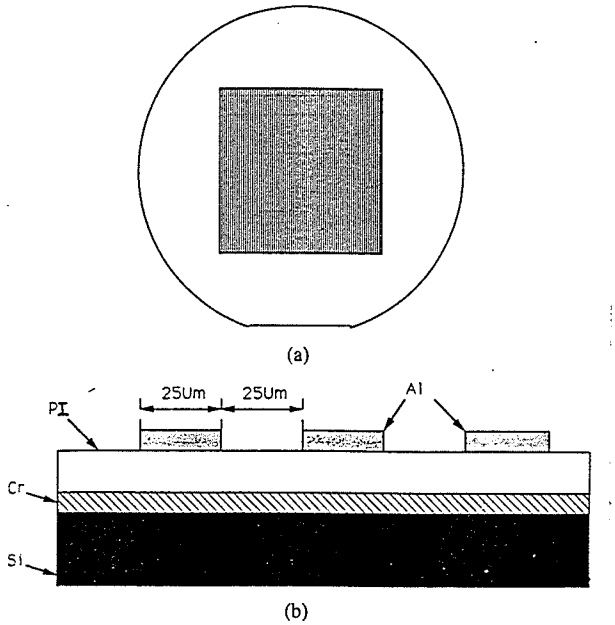

Figure 2.9: *(a) Top view of polyimide sensor devices. (b) Cross section of polyimide sensor device(after Schubert and Nevin, [50]).*

Chapter 3

Carrier Injection, Transport and Breakdown in Polyimide

As the polyimide has been considered as a promising material for microelectronics applications[1,2], a great deal of research has been carried out to investigate its electrical properties. Electrical properties such as electric conduction were usually studied under low fields (<500 kV/cm) [29,31]. To the best of our knowledge, conduction under high fields (>1MV/cm) has not been reported yet. Using the metal-polyimide-semiconductor (MPS) structure, we have investigated the carrier injection, transport and breakdown processes based on the current-voltage (I-V) and the capacitance-voltage (C-V) characteristics. By studying the relation between the injection current and the applied field, it has been confirmed experimentally that electric conduction is due to the Fowler-Nordheim type tunneling injection at high fields[52].

In this chapter, we present our new results on electric conduction and breakdown and our interpretation of these results in terms of the traps in the MPS structure.

3.1. Theory of Electric Conduction

A simple analysis for electric conduction in polyimide has been carried out. All the polymers including polyimide contain various kinds of unavoidable impurities and structural defects which form traps located in the energy band gap. The trapped charges are distributed in the polymers. The energy band diagrams for the case with the *p*-type silicon grounded and the gate biased at zero, negative or positive voltage are shown in Figure 3.1. In these diagrams, the image force is not shown because it has only a very small effect on the barrier height of the injecting contact(<5%). However, we have included this image force effect in our computation in section 3.4.

Since the work function of metal (Au) is smaller than that of the *p*-Si, some electrons will flow from the metal to the *p*-Si, creating a depletion region of width *W* in the *p*-Si as shown in figure 3.1 (a). Furthermore, donor-like traps near the polyimide/ *p*-Si interface or at the interface would also trap the holes helping the formation of a depletion region.

When the metal gate is negatively biased with a voltage sufficiently large as shown in figure 3.1(b), the metal-polyimide-*p*-silicon (MPS) system is in an accumulation mode. In this case, electrons will inject from the metal to the PI and holes will also inject from the *p*-Si to the PI. In this case both trapped electron charges and trapped hole charges tend to cancel each other their effect on the fields at the injecting contact. Thus under certain conditions, no ledge occurs.

When the metal gate is positively biased with a voltage sufficiently large, the operation of the MPS system would change its depletion mode to an inversion mode. In this case, because of the difference between the barrier height for electron injection and that for hole injection, electron injection from *p*-Si becomes dominant as shown in figure 3.1 (c). Thus the concentration of trapped electron charges would be higher at or near the PI/ Si interface probably because the trap concentration is higher near the interface[52]. There is a net negatively trapped charge with its centroid located at x_c measured from the PI/ Si interface.

The electrons injected from the injecting contact to the PI will be partly trapped in traps. The rate of trapping can be written as [53],

$$\frac{dn_t}{dt} = \frac{\sigma j(t)}{q}(N_t - n_t) \qquad (3.1)$$

where n_t and N_t are the filled and the total electron trap concentrations, respectively. σ is the effective trap cross section, j(t) is current density, and q is the electronic charge. If detrapping is assumed to be negligible, then N_t can be considered as the saturated concentration of the filled traps under a particular set of experimental conditions. If j(t) is due mainly to the Fowler-Nordheim (FN) type tunneling injection, then we can write [53],

$$j(t) = \frac{q[F_c(t)]^2 m}{16\pi^2 \hbar \Phi_B(t) m^*} \exp\{-\frac{4(2m^*[\Phi_B(t)q]^{3/2}}{3\hbar q F_c(t)}\} \qquad (3.2)$$

where $F_c(t)$ is the electric field at the injecting contact, $\hbar$ is the Planck's constant, m^* is the effective mass of the tunneling electron in PI and is assumed to be 0.5 m, and

m is the electron rest mass. $\phi_{BP}(t)$ is the barrier height. In the tunneling region, the injecting contact is not triangular if the image force lowering effect is taken into account. The image force lowering is given by[54],

$$\Delta\phi_B = \phi_{BP} - \phi_B = \sqrt{\frac{q^3 F_c(t)}{4\pi\varepsilon_{PI}}} \tag{3.3}$$

where ϕ_{BP} is the potential barrier height of the injection contact which is given by,

$$\phi_{BP}=\phi_m - \chi \tag{3.4}$$

ϕ_m is the work function of the electrode materials and χ is electron affinity of the PI. In case the injecting contact is at PI/ Si interface, the potential barrier height ϕ_{BP} is then given by,

$$\phi_{BP} =\phi_S - \psi_S - \chi \tag{3.5}$$

The electric field at the injecting contact can be written as:

$$F_c(t) = \frac{V(t) + \phi_{ms} + \psi_s(t)}{d} - \frac{qn_t(t)}{\varepsilon_{PI}}\left(1 - \frac{x_c}{d}\right) \tag{3.6}$$

where V(t) is the applied ramp voltage with the ramp rate of g (V/s), d is the thickness of the PI sample, ϕ_{ms} is the work function difference between the metal and the p-type silicon which is always negative because ϕ_s is always larger than ϕ_m , ψ_s is the surface potential and should be very small as compared to $|\phi_{ms}|$ and practically not sensitive to the magnitude of the applied voltage. n_t is the total concentration of the trapped electrons with the centroid at x_c.

From equation (3.6), the lowing of the field at the injecting contact ΔF due to the trapped electron charge qn_t is given by,

$$\Delta F = \frac{qn_t}{\varepsilon_{PI}}(1 - \frac{x_c}{d}) \qquad (3.7)$$

Where ε_{PI} is the permitivity of the PI. When the rate of the increase of the internal field due to the trapped electrons approaches the ramp rate of the applied field g, the quasisaturation begins to appear and persists until all of the traps are filled. The quasisaturation region appears as a ledge in the I-V characteristics of width ΔF_L which can be written as,

$$\Delta F_L = (qN_t / \varepsilon_{PI})(1 - x_c/d) \qquad (3.8)$$

The total current flowing in the sample consists of the displacement current and the Fowler-Nordheim tunneling current at high fields. At low fields, the displacement current is dominant. The total current can be expressed as,

$$I(t) = C_{PI}\frac{dV_a(t)}{dt} + Aj(t) \qquad (3.9)$$

where C_{PI} is the total capacitance of the PI film and A is the injecting contact area. The first term on the right side of equation (3.9) is the displacement current, and the second term is the injection current.

The I-V characteristics of the PI sample can be obtained by solving equations (3.1)-(3.9). Because of the non-linear nature of these equations, the computer

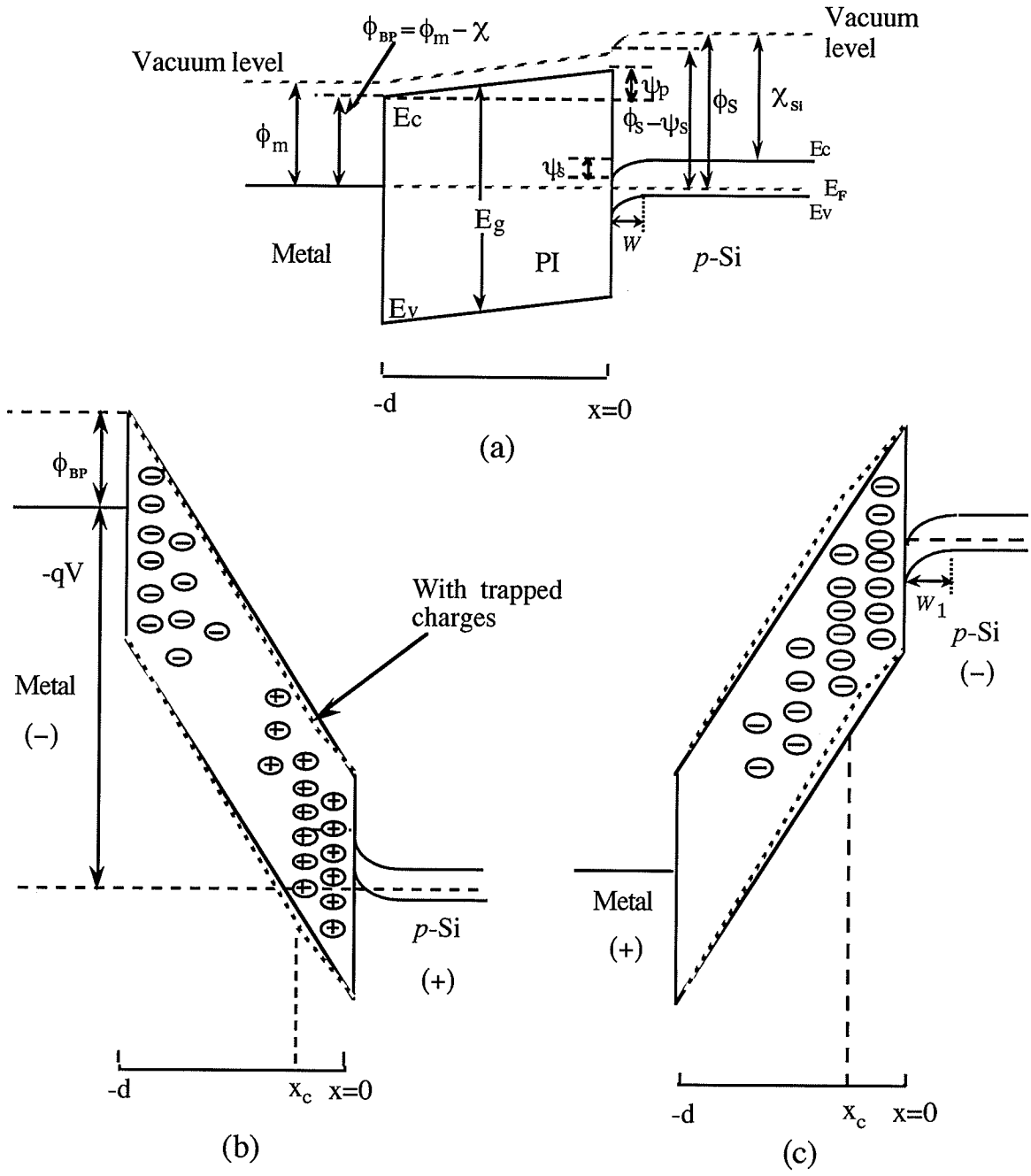

Figure 3.1: *Schematic energy band diagrams illustrating: (a) the potential barriers in the absence of applied voltage (b) the potential barrier with the presence of trapped electron and hole charges for the metal gate biased with a positive voltage (c) the potential barrier with the presence of trapped electrons charges for the metal gate biased with a negative voltage.*

program of Maple in conjunction with the fourth-order Runga-Kutta numerical method was implemented for the solutions of these equations.

It should be noted that as the trapping process goes on, each electron trapping will evolve an energy of the order of 2-5 eV depending on the trap energy levels for the large band gap materials. This energy, if not converted to light emission, will be dissipated in the materials in the form of breaking bonds and hence creating defects or traps according to the Kao's model [55]. At the fields close to the breakdown field, the conduction is filamentary[56]. A high current density filament may develop thermal instability and then create subsequently low density regions which provide long mean free paths for impact ionization thus leading to an abrupt increase in conduction current and breakdown[57].

To determine the type of carriers responsible for electric conduction, we used the C-V characteristics under varying biasing conditions. For *p*-type silicon substrate, the MPS system is in an accumulation mode when the gate is negatively biased and the measured capacitance is just the capacitance of the insulating film. When the gate is positively biased, the MPS is in a depletion mode if the voltage is not large enough to switch on an inversion mode. In this case, the overall capacitance of the MPS system is decreased. When the negative gate bias is sufficiently large, an inversion layer of minority carriers is formed at the *p*-Si surface. At the threshold voltage for the occurrence of an inversion layer, the overall capacitance becomes a minimum[58]. With an n-type silicon in the MPS system, the polarity dependence is just reversed, but the general characteristics remains unchanged.

At high fields charge carriers will be injected from the injecting contacts. Since the C-V characteristics depend strongly on the trapped charges near the PI/Si interface. These trapped charges (electrons or holes) will attract or repel coming charges depending on their polarity, which is reflected in the C-V hysteresis loop. The direction of C-V loop would indicate the type of the carriers injected from the injecting contact. If the injection is from the metal, some charge carriers must be trapped in the PI bulk and at the PI-Si interface, thus affecting the C-V curves. For carrier injection from the metal, only when the metal gate is at positive polarity, holes will be injected and produce a positive trapped charges near the metal/ PI interface and in the PI bulk. This trapped holes cause the system operating in a depletion mode, thus the overall capacitance is reduced. The decrease in capacitance gradually becomes small as the positive gate voltage gradually swings to the negative polarity as shown in figure 3.2 (a). When the gate voltage reaches a maximum values, electron injection ensues and this will neutralize some of the trapped hole charges. As the gate voltage swings toward the positive polarity again, a net negatively trapped charge becomes dominant, leading to the formation of a hysteresis loop as shown by the solid lines. For an ideal situation in which there is no trapped carrier charges and no injection from the metal, the C-V curve is represented by dashed line. If the metal can inject electrons, but not holes, then the dashed line and solid line 2 will form the hysteresis loop. On the other hand, if electrons can be injected and holes can not, the hysteresis loop will be formed by the dashed line and solid line 1.

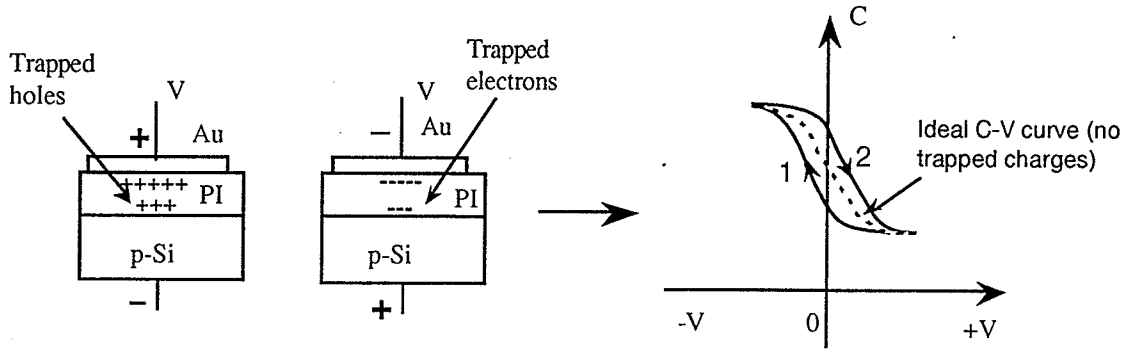

(a) Carrier injection from Au metal

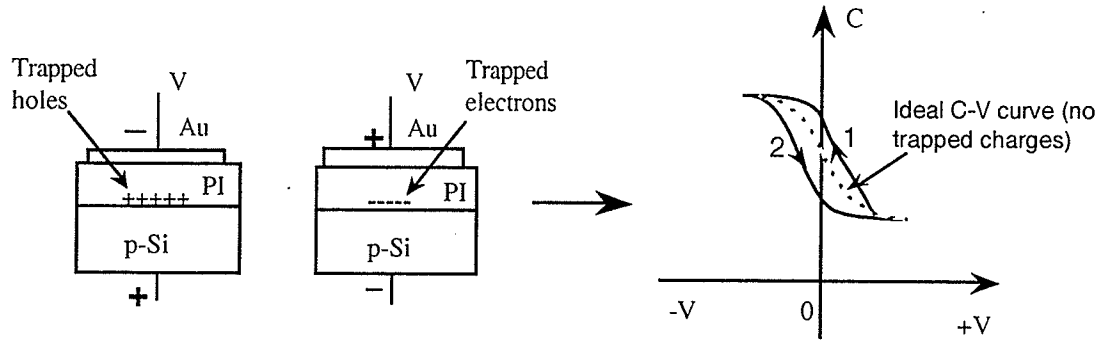

(b) Carrier injection from p-Si

Figure 3.2: *(a) Charge injection from the metal only (a) and from the p-silicon only (b), and the corresponding C-V curve.*

For carrier injection from the *p*-type silicon, the direction of the hysteresis loop is just opposite to that for carrier injection from the metal. From the direction of the hysteresis loop, we can determine the nature of the injected carriers, electrons or holes, and also whether the injection is from metal or silicon.

3.2 Experimental Techniques

The polyimide (PI) films used for this investigation were fabricated using Dupont PI2556 synthesized from benzophenone tetracarboxylicacid dianhydride (BTDA) and oxydianiline (ODA). The synthesis changes the structure of the BTDA-ODA poly(amic acid) to the structure of the polyimide as shown in figure 3.3. The substrates were *p* -type, <100> oriented, 30-60 Ω-cm silicon wafers. All substrates

were carefully cleaned using the RCA method with 10^6 Ω-cm distilled water [59]. After that, substrates were dipped in a reduced HF/ H_20 solution (1:100 cm^3) to remove the native oxide on the surface, and then the PI2556 solution was spin-coated on the substrate surface to form the PI film. The PI film samples were thermally cured at 120°C in air for 30 minutes and then further cured at 350 °C in nitrogen for another 30 minutes unless otherwise noted. All samples at this high curing temperature were considered to have a 100% imidization [15]. In this investigation, the PI film thickness is about 6500 Å measured with the Dektak surface profile unit and checked by ellipsometry. All samples were stored in the desiccator for one day before test. For electrical measurements, a thick aluminum film was vacuum-deposited on the silicon surface to form the bottom electrode, and gold electrodes of 1.5 mm in diameter each were deposited on the PI film surface through a shadow mask to form metal-polyimide-semiconductor (MPS) capacitors. Figure 3.4 shows the preparation procedure sequences for the fabrication of MPS capacitors. The techniques used for the measurements of the ramp current-voltage (I-V) and high frequency (1 MHz) capacitance-voltage (C-V) were the same as those reported earlier [60,61]. The experimental setup is shown in figure 3.5. All the measurements were performed at room temperature (22° C).

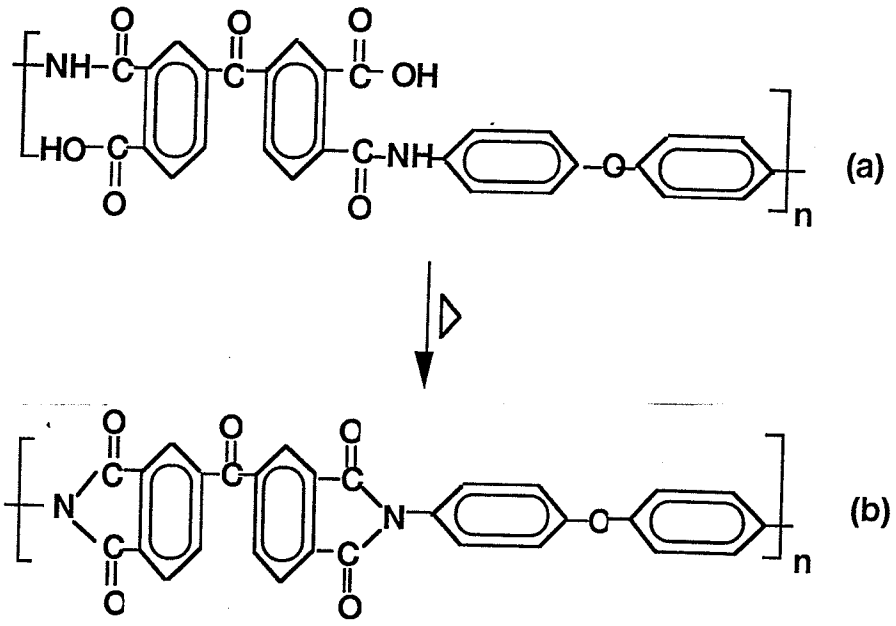

Figure 3.3: *Structure of (a) BTDA-ODA poly(amic acid) and (b) polyimide*

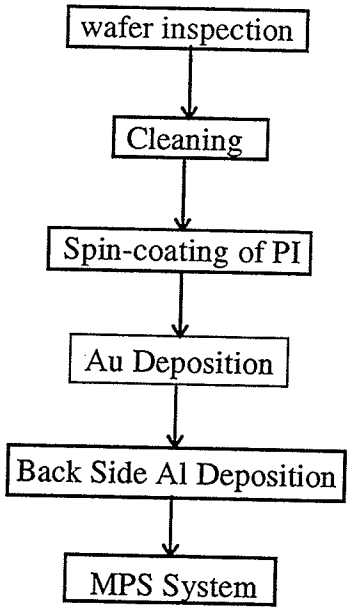

Figure 3.4: *Preparation procedure for MPS system sample*

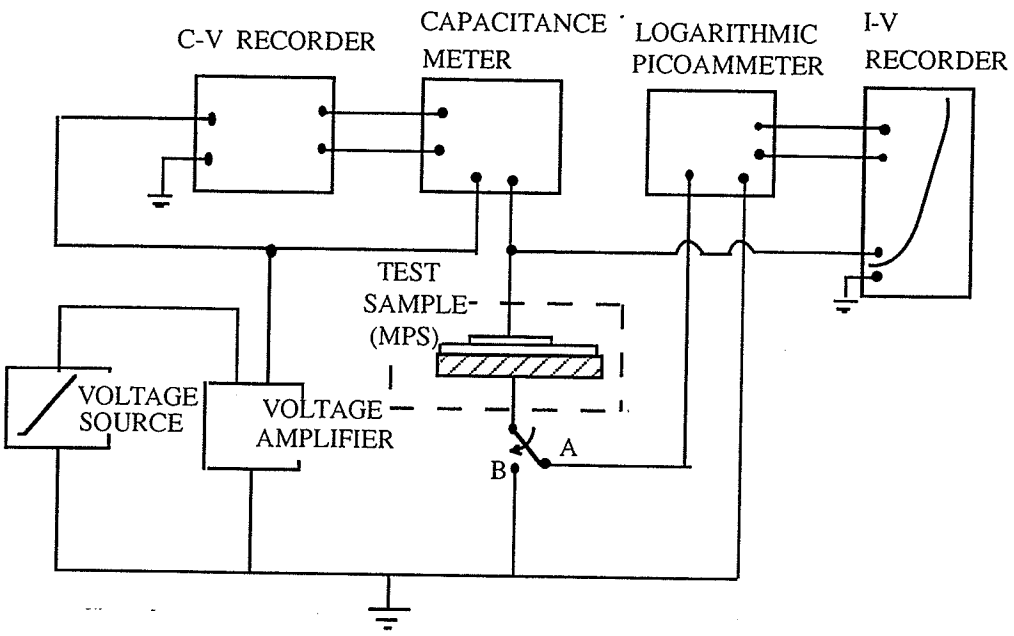

Figure 3.5: *Experimental setup for the measurements of the ramp current-voltage (switch on A) and capacitance-voltage (switch on B) characteristics.*

3.3 I-V and C-V characteristics

3.3.1with the Au gate electrode negatively biased

When a linear negative voltage ramp is applied to the gate, the current I versus the voltage V characteristics of the MPS system are shown in figure 3.6. The total current I was plotted as a function of average field F(=V/d). The current remains almost constant up to the threshold field where the charge carrier injection begins. The displacement current is C(dV/dt) and is dominant in the low field region I, where C is the overall capacitance of the MPS. The lower the ramp rate, the lower is the displacement current because it depends on dV/dt. The threshold field for the carrier

injection is about 1.4 MV/cm. In the high field region II, the current increases rapidly with increasing field following closely the Fowler-Nordheim relation. However, the I-V characteristics in the high field region II depend also on the ramp rate. The lower the ramp rate, the smaller is the current at the same fields, indicating that with a slower ramp rate, more carriers will be trapped resulting in the creation of a higher internal field opposite to the applied field, thus causing the reduction of the injection current.

The C-V characteristics of the Au-polyimide-Si (*p*-type) system always exhibits a hysteresis behavior as shown in figure 3.7. The curve 1, recorded when the bias sweep starts at zero and moves towards negative voltage, can be considered as the indication of the initial concentration of the trapped charges in the polyimide film. The curve 1' is traced when the bias sweep voltage decreases from a negative value to zero. The curve 1-1' forms one sweeping cycle, and curves 2-2', 3-3' are second and third sweeping cycle, respectively.

From the first sweeping cycle, it can be seen that the depletion region has been formed near the interface of PI film even when the biasing voltage is zero and also the return loop shifts to a more negative voltage. This is in the opposite direction if it is considered to be due to the ionic charges moving in the polyimide. That is, when the voltage increases, more mobile negative charges would be driven towards the PI-Si interface, and more positive mobile ionic charges be driven away from the interface and move toward the negatively biased gate. This would leave more negative charges near the PI/Si interface which would reduce the width of the depletion layer and make the overall capacitance higher. This implies that more

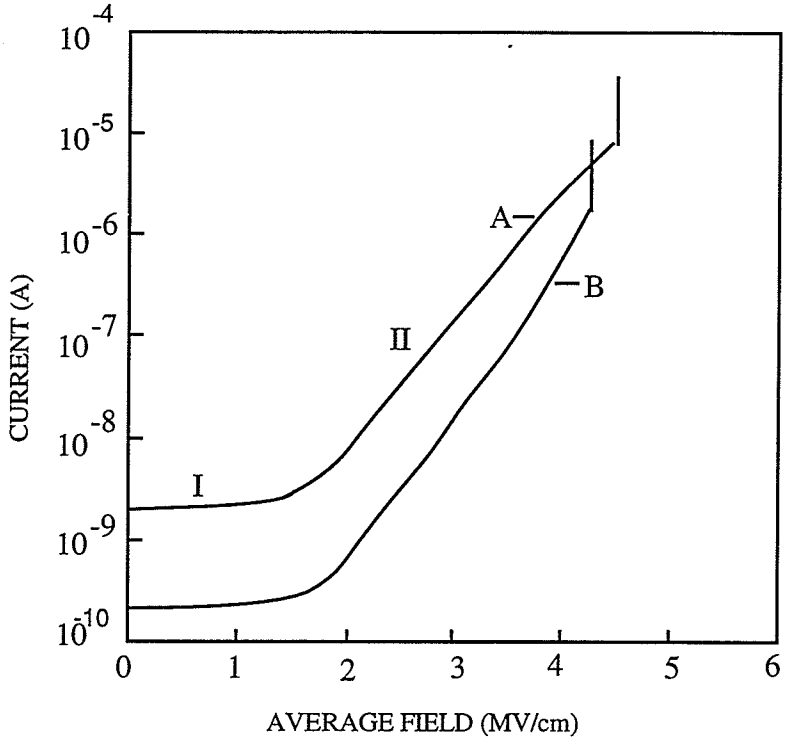

Figure 3.6: *Current-average field (I-Fg) characteristics with different ramp rate. (A) ramp rate: 0.26 MV cm $^{-1}$ sec $^{-1}$ and (B) ramp rate: 0.026 MV cm $^{-1}$ sec $^{-1}$.*

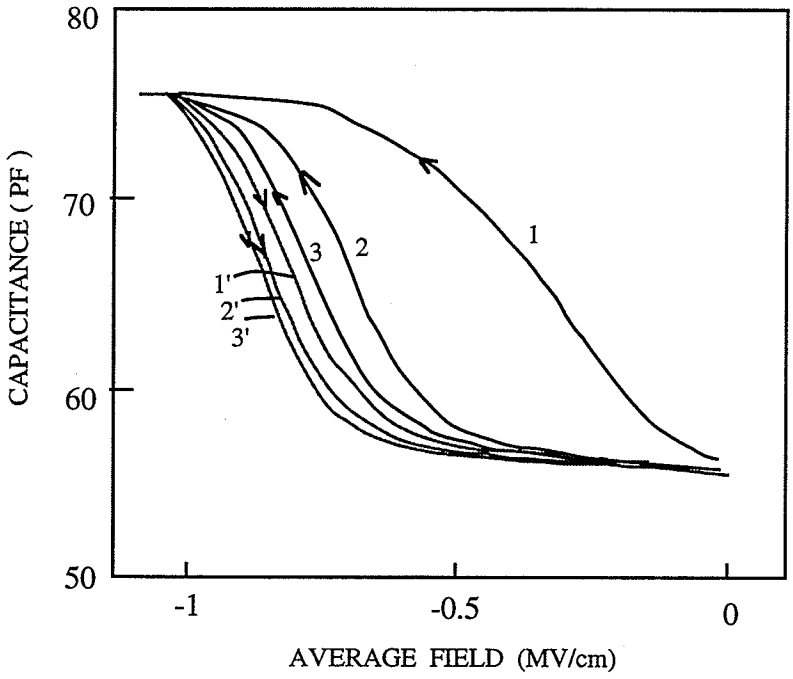

Figure 3.7: *Typical C-V characteristics of the MPS system.1-1', 2-2', and 3-3' represent the first, second, and third voltage sweeping cycles.*

negative charges at or near the PI/Si interface would shift the C-V curve to more positive voltage value. However, this is not the case as shown in figure 3.7. The experimental results show that the C-V curve is shifted to the negative direction during the return loop. Therefore, ionic charge is not the reason for the observed hysteresis. The C-V hysteresis of the MPS system indicates that a positive charge layer near the PI/Si interface has been built up during the voltage sweep. During the return loop, the presence of positive charge layer leads to a shift of C-V curve to a more negative voltage. We believe that the positive trapped charge is due to the surface states[62-65] at the PI/Si interface. Charge carriers can be easily transferred from Si into the bulk and the PI/Si interface by a tunneling mechanism with or without applying electric field. Further tunneling is impossible due to the large distance between the interface states and bulk states[66]. In general the trap concentrations near the PI/Au and PI/Si interface are much higher than that at the middle of the PI. The polyimide may have a variety of coexisting donor and acceptor like states in the bulk and as well as at the PI/Si interface .

After the first C-V hysteresis loop was measured , then the second and third were immediately followed. From figure 3.7 , it can be seen that the C-V loops shift to the left of the first one. This is consistent with the assumption that a positive charge layer was formed during the voltage sweep and part of holes were released during the return loop. Furthermore, the hysteresis loop itself gradually diminishes in the following cycles, indicating that the filling of surface states may have reached a dynamic equilibrium under the same sweep swing.

While the trapped hole space charge suppresses the effective field at the hole injecting contact and hence the hole injection, it enhances the effective field at the electron injecting contact, and the electron injection may become possible. This is in fact the case of double injection since both types of carriers can be injected from both injecting contacts. As some of electrons move toward the *p*-silicon, the bulk traps in the PI film are gradually filled starting from the Au gate toward the *p*-Si. Trapped electrons will form a negative trapped charge which then retards the on-coming electrons and this is an opposite effect caused by trapped holes. So the overall space charge effect in polyimide may be reduced and this is the reason why I-V characteristics in figure 3.6 follow closely to the Fowler-Nordheim relation.

We used C-V measurements coupled with the I-V measurements to study the trap behavior. In figure 3.8, after a Virgin MPS sample was stressed with a first cycle of linear voltage ramp at the ramp rate of 0.026 MV cm^{-1} sec^{-1} until it reached 1.2 MV/cm, it was held there for ten seconds. In the second, third and fourth cycle, the electric fields reached 2.2 MV/cm, 4.0 MV/cm and 4.2 MV/cm respectively and were held there for ten seconds each as shown in figure 3.8 (a). It can be seen that the I-F curves shift to the right of the first one. The current at the holding point also decreases with the time indicating the buildup of the space charge. Further more, for the third and fourth cycles , the current at the holding points decreases less with time. This implies that electrons are the dominant carriers injected from the Au electrode. This is further supported from the results of C-F measurement as shown in figure 3.8 (b). The C-F curve after the first cycle of ramp voltage stressing moves to the left of

the virgin sample's indicating the buildup of positive space charge near or at the PI/Si interface after the stressing at 1.2 MV/cm for ten seconds. However, the C-F curves after stressing at 2.2 MV/cm, 4.0 MV/cm and 4.2 MV/cm for ten seconds move back to the right side of curve 1. This shows that the effect of trapped holes on C-V characteristics is reduced by the injected electrons from the Au electrode when the applied field is higher than the threshold field (1.4MV/cm). The C-F curves even shift to the right of that for the virgin sample after several cycles of high field stressing. This implies the presence of a large concentration of trapped electrons in the PI sample which is caused by the injection of the electrons from the Au electrode at high fields.

The electric conduction and the average breakdown strength depend on the ramp rate of the applied voltage ramp. The slower the ramp rate, the lower are the conduction current and the breakdown strength as shown in figure 3.6. The lower ramp rate results in more carriers to be trapped and thus a higher internal field to be created thus reducing the conduction current. And also, the longer the time for the current flow through the sample, the more is the heat generated to cause thermal instability. This is why the lower the ramp rate, the smaller is the breakdown strength.

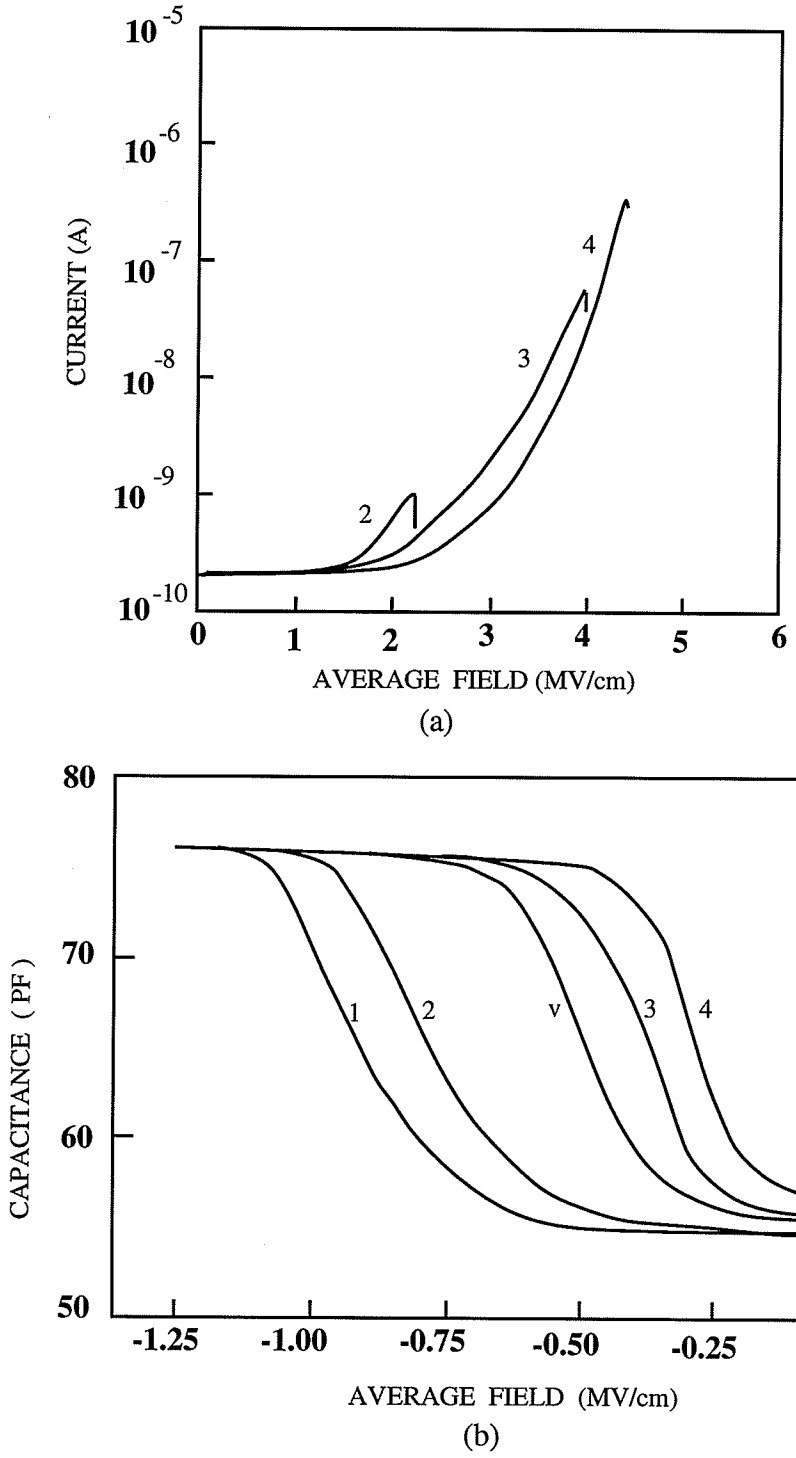

Figure 3.8: *Effects of the ramp voltage stressing on (a) the I-F characteristics and (b) the corresponding C-F characteristics for the virgin sample v and after 1st, 2nd, 3rd, and 4th cycle of stressing with the average fields of 1.2MV/cm, 2.2 MV/cm, 4.0 MV/cm and 4.2 MV/cm. Gate polarity : negative, ramp rate: 0.026 MV cm $^{-1}$ sec $^{-1}$.(the first I-V ramp not shown due to the low conduction current)*

3.3.2 With the gate Au electrode positively biased.

When a positive voltage is applied to the Au gate electrode, the I-V characteristics of the MPS systems always exhibit a ledge as shown in figure 3.9. For the first cycle the threshold field is about 1.4 MV/cm. During the first cycle, most of traps may have been filled and after the first cycle, some trapped electrons remain trapped and the internal field created by those trapped electrons oppose the applied field. This is why a higher field is required to start the FN tunneling injection, or in other words, the threshold field for the FN tunneling injection is increased from 1.4 MV/cm to about 2.0 MV/cm for the second cycle and even higher for the third cycle. This phenomenon indicates that there is a net negatively trapped charge building with its centroid near the injecting PI/Si contacts, and that this centroid tends to move more closely to the contact after each stressing cycle. However, no ledge has been observed for the case with the Au gate electrode negatively biased no matter how many stressing cycles have been applied to the MPS system.

We used the same method described in the previous section to study the conduction process when the gate electrode is positively biased. The measurements of I-V characteristics is coupled with C-V characteristics were used to determine the nature and transport of charge carriers. After the C-V characteristics of a virgin MPS sample have been measured, the sample was stressed with a first cycle of linear voltage ramp at a ramp rate of 0.026 MV cm^{-1} sec^{-1} until it reached 1.2 MV/cm, it is then held there for 10 seconds. The C-V measurement after the 1st cycle stressing showed that there is negative trapped electron charge near the PI/Si injecting contact

as shown in figure 3.10 (b).Using the same procedure, when the 2nd, 3rd and 4th stressing cycles reached 1.5 MV/cm, 2.1 MV/cm, and 3.8 MV/cm respectively, they were held there for ten seconds each. Right after each of these stressing cycles, C-F characteristics were measured with a sweep field from + 0.5 MV/cm to -0.75 MV/cm, which is below the threshold voltage for FN injection. During the second I-V ramp cycle, the current at the holding point decreases gradually to the value of the displacement current (i.e. approaching zero injection current) as shown in figure 3.10(a). This implies that the internal field is large enough to reduce the effective field at the electron injecting contact to a value below the threshold field for electron injection. It can be seen from figure 3.10(b) that all the C-F curves after stressing cycles shift to the right of the C-F curve for the virgin sample and that the higher the stressing field, the more in the shift to the right. This indicates that at high fields the MPS system is in strong inversion mode and therefore the current and the negatively trapped electric charges are due to the FN injection from *p*-silicon. The internal field created by the trapped electron charge depends on both the concentration and the centroid of the total net trapped charges. When the rate of the increase of the internal field approaches the ramp rate, the current becomes saturated to form a ledge in the I-V characteristics as shown in figure 3.9. The current in the first ramp cycle is much lager than that in the second and third ramp cycle at the same electric field in the high field region II indicating clearly the buildup of a negative space charge. However, in region III, the ledge current appears almost at the same location for the 1st, 2nd, and 3rd ramp cycle. This implies that the detrapping could be important at high fields,

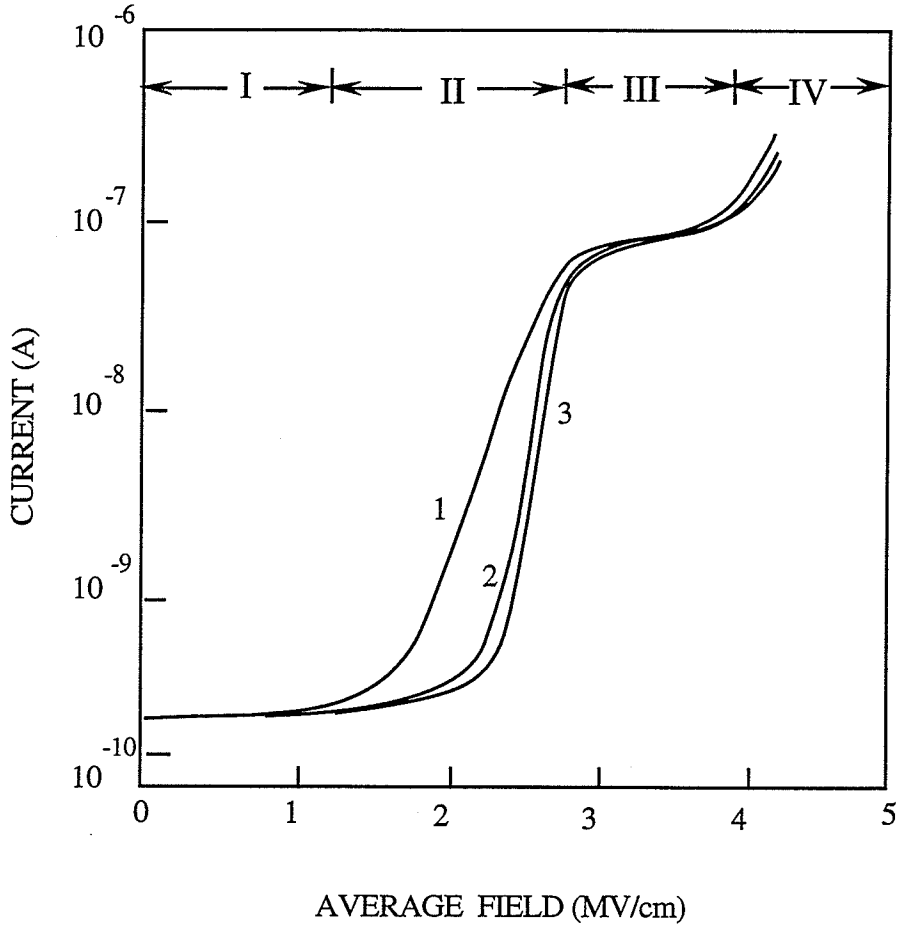

Figure 3.9: *The I-V characteristics of MPS structure with positive polarity on the Au electrode. Ramp rate: 0.026 MV cm $^{-1}$ sec $^{-1}$. 1, 2, 3, are the first, second, and third ramp cycle respectively*

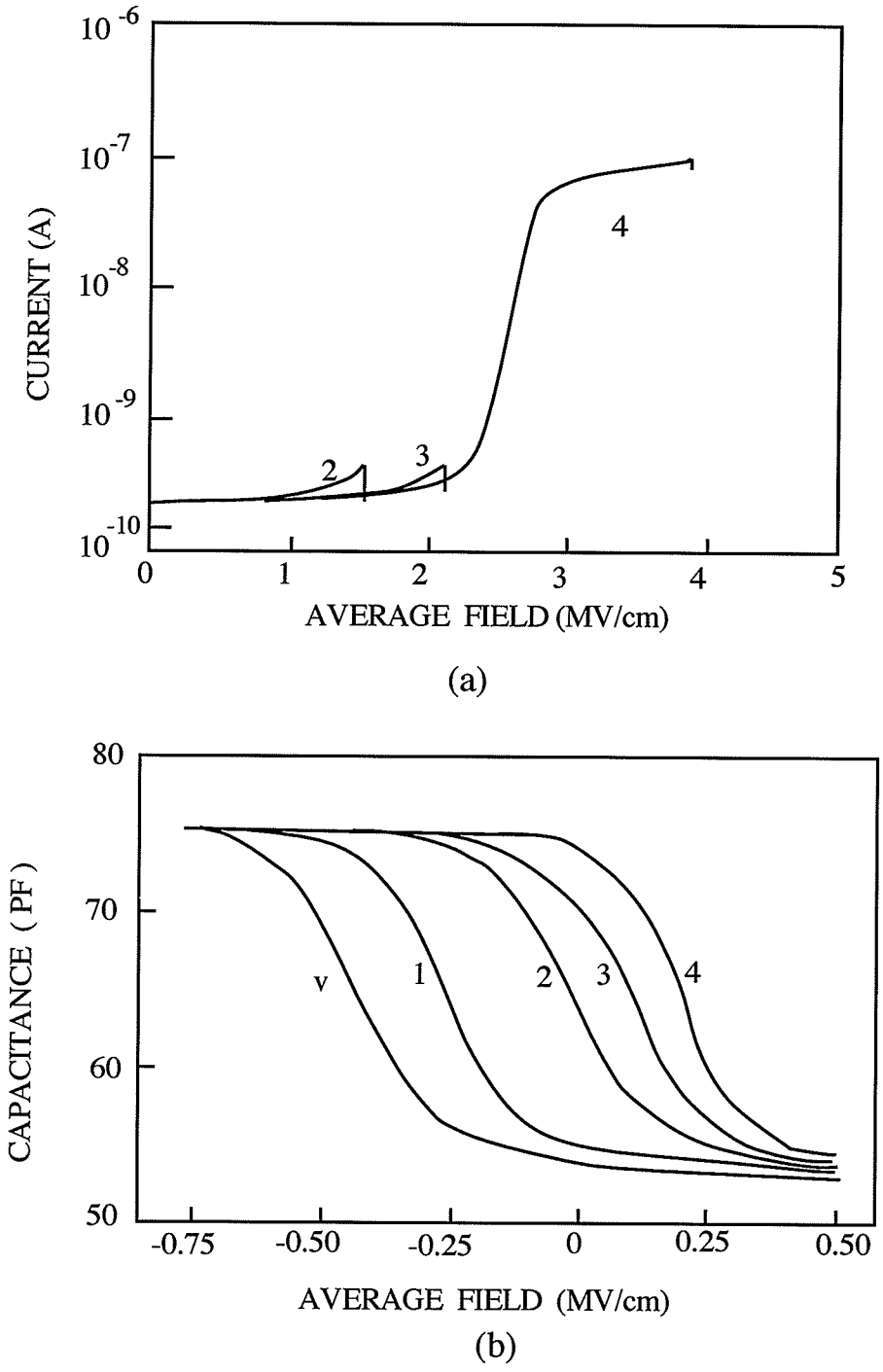

Figure 3.10: *Effects of the ramp voltage stressing on (a) the I-F characteristics and (b) the corresponding C-F characteristics for the virgin sample v and after 1st, 2nd, 3rd, and 4th cycle of stressing with average stressing fields 1.2 MV/cm, 1.5 MV/cm, 2.1 MV/cm and 3.8 MV/cm for ten seconds. Gate polarity: +, ramp rate: 0.026 MV cm $^{-1}$ sec $^{-1}$ (the first I-V ramp not shown due to the low conduction current).*

possibly due to the Poole-Frenkel effect[67]. It is likely that the hole injection from Au electrode is negligibly small, otherwise, it would enhance the electron injection at the cathode and the ledge phenomenon would not be observed. However, up to this moment we are still not clear why hole injection is small. The barrier height for electron injection may be slightly smaller than that for hole injection. The other reason may be due to the low mobility of holes in polyimide. It has been reported that polyimide has a very narrow valence band width about 0.25 eV[68]. Specific data about electron and hole mobility are still not available in the literature.

In region IV, we can consider that all traps have been filled and the conduction may be due to double injection, i.e. the hole injection from the Au anode becomes important.

3.4 Numerical Analysis of the Electrical Conduction Process.

We used the computation program of Maple in conjunction with the fourth order Runge-Kutta numerical method[69] for the solutions of equations from 3.1 to 3.9. The details of the computation are given in Appendix. The physical parameters used for the computation are as follows,

Electron trap capture cross section: $\sigma=10^{-16}$ cm^2 [54]

Relative permittivity of PI (dielectric constant): $\varepsilon_{PI}/\varepsilon_0=3.4$ [15, 29]

Potential barrier height at the injecting contact: $\phi_{BP}=3.8$ eV [15, 61]

Thickness of the PI film: $d_{PI}=6500$ Å

Area of electron-injecting contact: $A=1.77\text{x}10^{-2}$ cm^{-2}

Ramp rate of the ramp voltage: g=1.7 V/s

First we want to see the effect of the trapped electrons per unit cross section area of the sample on the I-V characteristics. To use the computed I-V curve to simulate our experimental I-V curve, we choose $x_c = 0$. This means the centroid of the trapped electron concentration is near or at the electron injection PI/Si contacts, and the total effective electron trap concentrations ranging from $N_t=2x10^{13}$ cm^{-2} to $N_t=5x10^{13}$ cm^{-2}. The computed I-V curves are shown in figure 3.11. The general shape of these curves is similar to the experimental one shown in figure 3.9. On the basis of the comparison between figure 3.9 and figure 3.11, the total traps of the PI sample is of the order of $4x10^{13}$ cm^{-2}. Of course, the trap concentration depends so much on the preparation of the samples. However, this trap concentration value is reasonable.

We have also studied the effect of the location of the centroid. In this computation, we choose $N_t = 4x10^{13}$ cm^{-2} and their locations of x_c , that is $x_c = 0$ (at or near the injection PI/Si contact), $x_c = d/2$ (at the middle of the sample) and $x_c = d$ (at or near the opposite Au electrode). The computed curves are shown in figure 3.12. By comparing these curves with figure 3.10, we can say that the centroid of the negative trapped electron charge is located near the PI/Si contact.

From figures 3.11 and 3.12. It can be concluded that for the occurrence of a ledge in the I-V characteristics, the centroid of the trapped charge must be near the current injecting contact. If x_c is not close to the injecting contact, the trap charge must be large enough to make the rate of the increase of the internal field created by the trapped charge approaches the ramp rate of the applied field.

It should be noted that the above simulation may not be strictly applied when the location of the trapped charge is very close to the PI/Si interface or when the distance is less than the barrier width for electron tunneling because the influence of the trapped charge on the current becomes diminished under such a condition. Therefore, the value of N_t should be interpreted as an equivalent trap concentration as seen from the injection contact for the FN tunneling injection. The actual trap concentration may be higher.

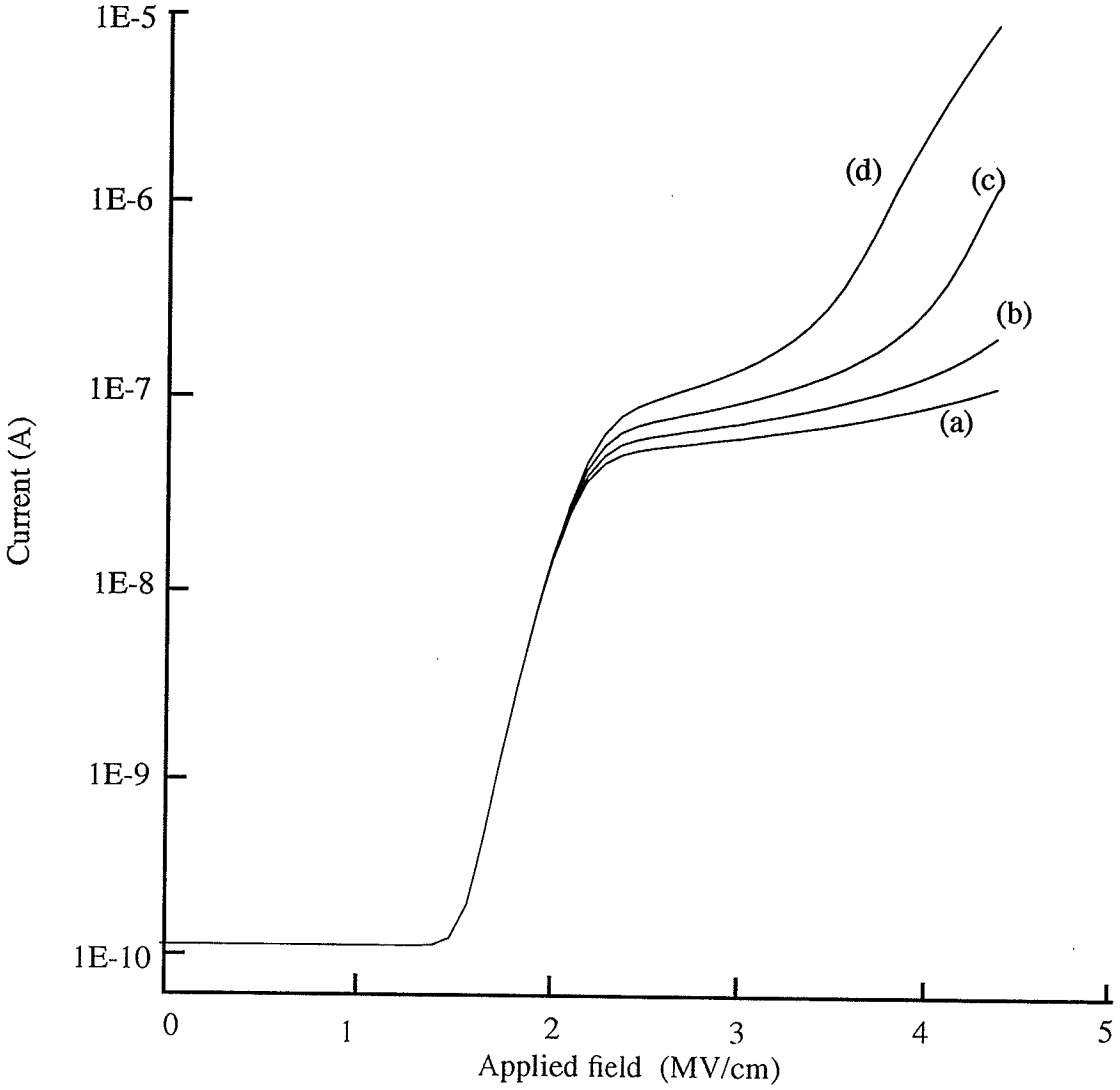

Figure 3.11: *Computer simulation results for the I-F characteristics with the Au gate electrode positively biased with a ramp voltage of the ramp rate 0.026 MV cm^{-1} sec^{-1} for the sample with the centroid of the trapped charge $x_c = 0$ and concentration (a) N_t : $5x10^{-13}$ cm^2 (b) N_t : $4x10^{-13}$ cm^2 (c) N_t : $3x10^{-13}$ cm^2 (d) N_t : $2x10^{-13}$ cm^2.*

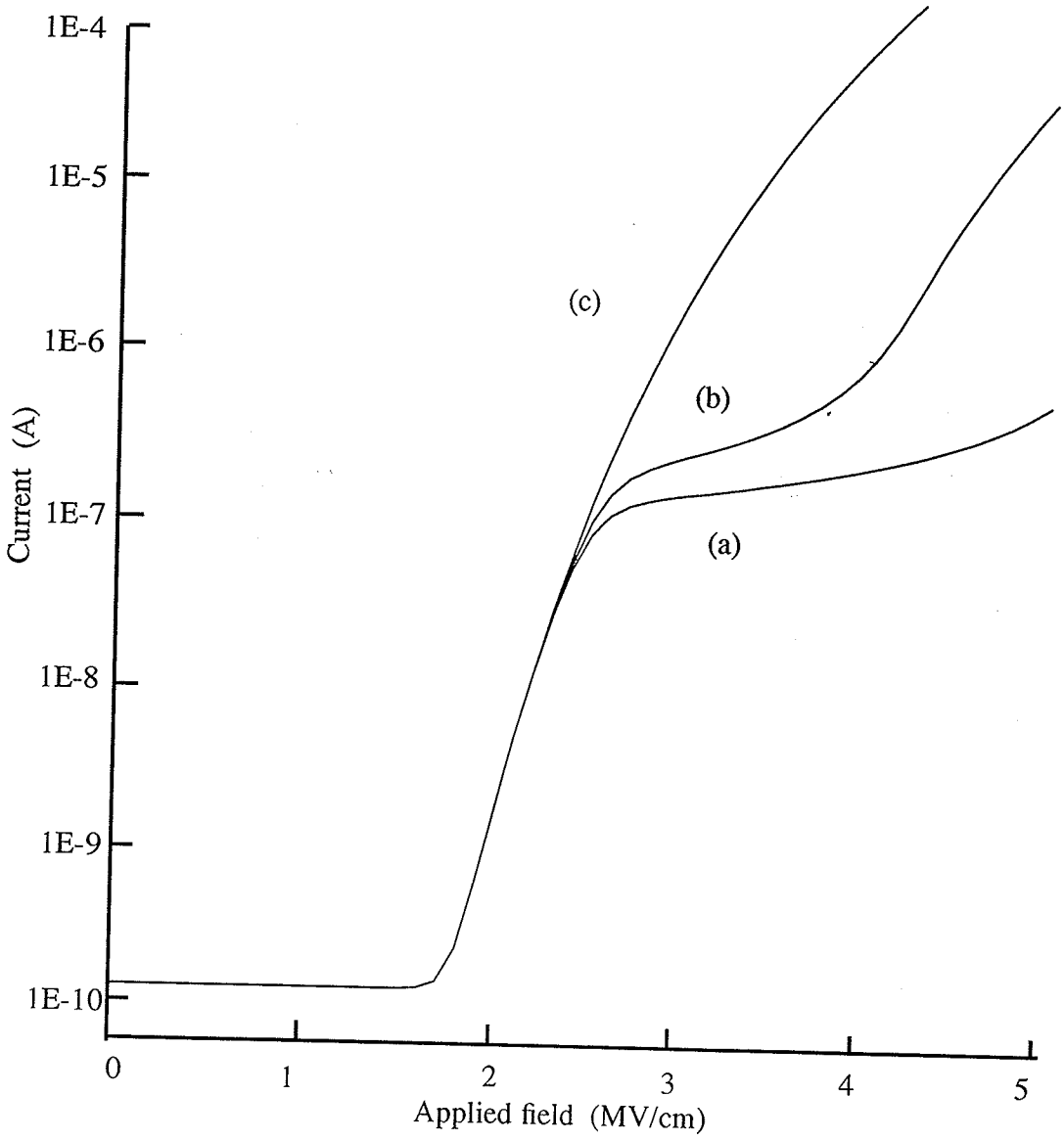

Figure 3.12: *Computer simulation results for the I-F characteristics with the Au gate electrode positively biased with a ramp voltage of the ramp rate 0.026 MV* cm^{-1} sec^{-1} *for the sample with* $N_t = 4x10^{-13}$ cm^2 *and the centroid located at (a)* $x_c = 0$ *(b)* $x_c = d/2$ *(c)* $x_c = d$.

3.5 Effects of humidity on Electric Properties

Water molecules absorbed in solids have a large dipole moment which would affect the electrical properties. The hygroscopic nature of PI results in degradation of its chemical and electrical properties [36]. From a practical point of view, the influence of humidity on electric properties, especially conductivity and breakdown strength, is important in the development of devices and new materials.

Aluminum (Al) electrode was vacuum deposited on a *p*-type (30-60 Ω.cm) silicon substrate to form the bottom electrode because Al has better adhesion to the PI film than silicon to the PI film. After PI had been deposited on the Al surface, a thin Au electrode (~300 Å) was vacuum deposited on the top of the PI film to form an MPM system. To ensure a good electrical contact a thick Al layer was also deposited on top of the gold electrode.

Measurements of the breakdown strength were carried out in a glass chamber at room temperature. We used the same method for measuring the I-V characteristics. The voltage was increased at a ramp rate of 1.7 V/s until the occurrence of breakdown. Each experimental point represents the average value of 10 measurements.

The humidity in a glass humidifying chamber was controlled by adjusting the temperature of the deionized water (10^8 Ω cm) and the pumping the vapor out of the chamber by a humidity controller as shown in figure 3.13. It took approximately 5 minutes for moisture absorption to reach it equilibrium for each humidity level and measurements were taken after the steady equilibrium condition has been reached.

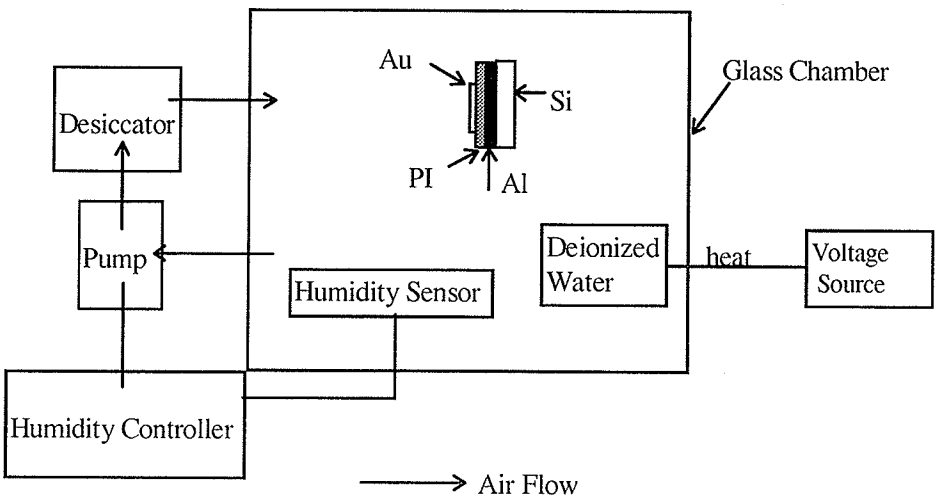

Figure 3.13 *Schematic diagram of the MPM structure and humidity control system*

The variation of capacitance with humidity is shown in figure 3.14. The capacitance is strongly dependent on humidity. The capacitance is also dependent on the medium in which the PI samples were cured. The change of the capacitance is attributed to the large dipole moment of water molecules absorbed inside the PI film. The film cured in air absorbed more water than those cured in the nitrogen. This is probably because of the oxidation of polyimide in the presence of oxygen at high temperature of 350 °C. Melcher *et al* [41] have reported that water molecules are bonded to two carbonyl oxygen atoms of two polyimide chains by two hydrogen bonds. Oxidation of PI is mainly the reaction between carbon and oxygen to form the carbonyl groups, which tends to increase the moisture absorption.

The conduction current were measured as a function of applied field with the ramp rate of 0.026 MV cm^{-1} sec^{-1} for two humidity levels, 65% RH and 20% RH. The results has shown in figure 3.15. The presence of the moisture inside the PI film has a marked effect on the I-V characteristics. The current is higher by several orders than the PI film without water content. This binding of water molecules makes it easier for carriers to tunnel from chain to chain at high electric fields.

The dependence of breakdown strength on humidity is shown in Figure 3.16. Since both the breakdown strength and the conduction current are dependent on humidity. It is therefore reasonable to assume that the decrease in breakdown strength is associated with the increase in conduction current. The increase in current causes an increase in temperature and in turn promotes the current buildup. Such a feedback process, is essential in thermal breakdown. It has been reported that the breakdown strength of polyethylene terephthalate films decreases by 2-3 MV/cm when the conductivity increases by 2-3 orders of magnitude in the thermal breakdown region[70]. The prebreakdown current increases rapidly at about 1 ms prior to final breakdown in PI, indicating the thermal breakdown process [36]. Nagao, *et al* [27] have reported that on the basis of the thermographs about the dynamics of temperature rise of the heated spot until breakdown, only one spot was predominant just prior to breakdown. They have also observed the breakdown spots in ordinary self-heating breakdown under microscope, the size of these spots in PI is distributed in the range of 1-10 μm in diameter. By assuming that the diameter of the breakdown channel is 10 μm. The energy dissipated per volume is

$$W=4VI/\ (\pi r^2 d) \qquad (3.1)$$

where r is the diameter of the current channel and d is the thickness of the film. From the measurements at the breakdown point with humidity 20% and 65%, the energy stored in the filament could reach 2.7 MW/cm^3. This is large enough to cause the thermal instability. We believe that destructive breakdown is caused by thermal destruction.

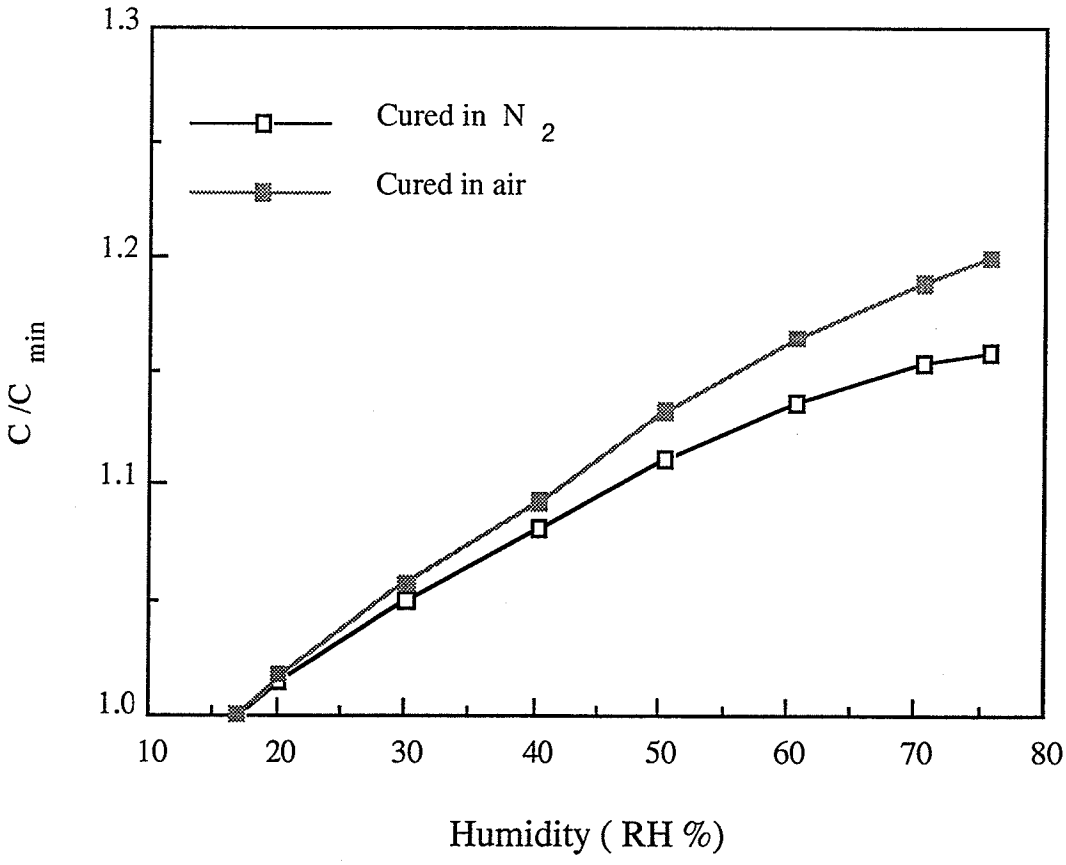

Figure 3.14: *Normalized capacitance change vs. humidity for polyimide cured in air and in nitrogen.*

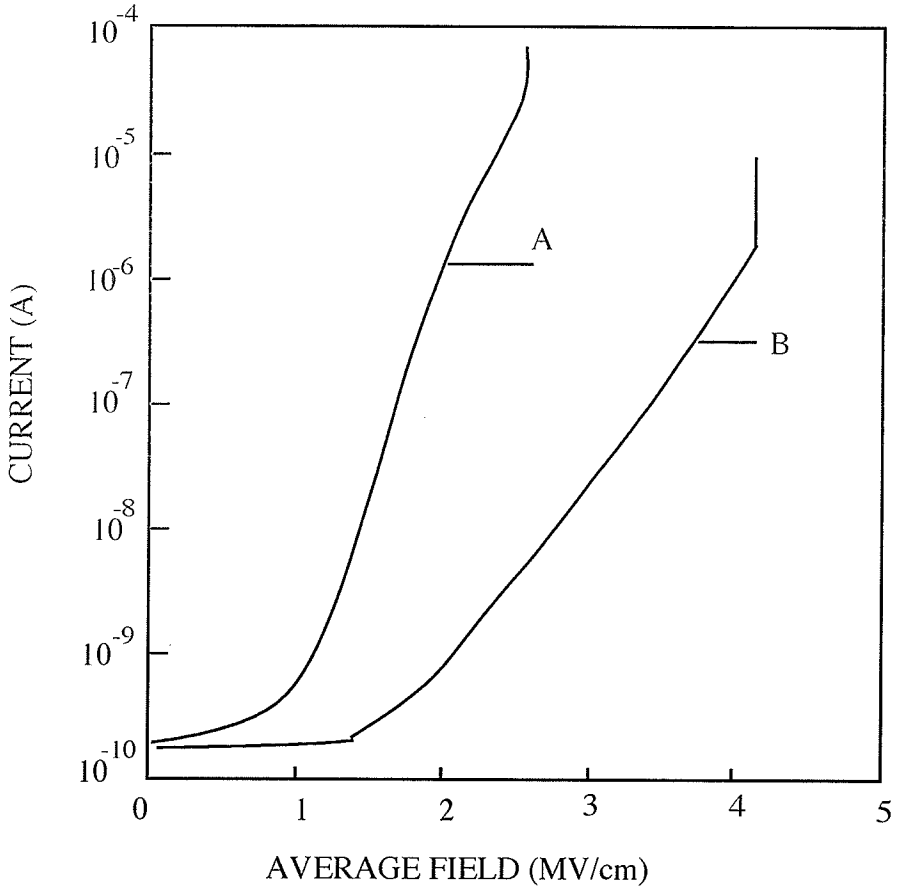

Figure 3.15: *I-V characteristics for the gate electrode negatively biased under humidity level (A) 65% RH and (B) 20% RH. Ramp rate: 0.026 MV cm $^{-1}$ sec $^{-1}$*

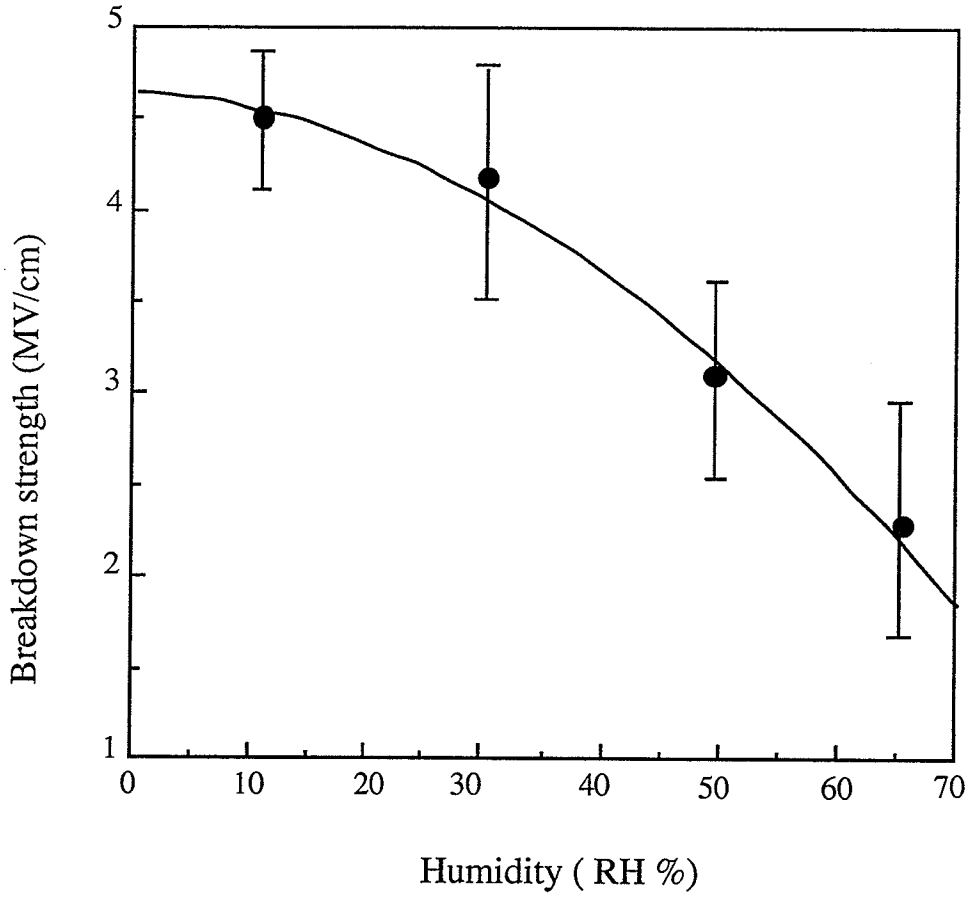

Figure 3.16: *Variation of breakdown strength of PI films with humidity. Ramp rate: 0.026 MV cm $^{-1}$ sec $^{-1}$.*

Chapter 4

Transient Photoconduction in Polyimide

Electric conduction in insulating polymers is of technical importance. A great deal of work has been done on this subject in the past three decades, but the mechanism of electrical transport in the polymers is still far away from full understanding. This arises largely because the dc dark conduction results measured under various conditions of temperature, electrical stress and ambient medium can be interpreted in a number of ways, especially when the experimental uncertainties and the generally poor reproducibility among specimens are taken into account [71,72]. Furthermore, the long time decay of the charging and discharging current in such materials makes it difficult to compare results obtained from different laboratories. It has been reported that the dark charging current and the photocurrent in polyethylene are independent of each other [73]. However, it can be imagined that the photocurrent measured after the charging current had reached its quasi-steady-state value would reveal the role played by the electron-filled traps in the electrical transport process. Tahira and Kao [74] were the first to report the strong dependence of the photocurrent on the magnitude of the dark charging and discharging current. They

measured the photocurrent transient during the period of dark charging and discharging current. In this chapter, we present some results of the photocurrent transient under low and high electric fields during the period of dark charging and discharging current.

4.1 Experimental Techniques

The method of preparing polyimide films is same as that described in chapter 3, but for this investigation we use an Au-polyimide-Al (MIM) structure. We first deposited a thick layer of aluminum on the Si wafer used as the bottom electrode prior to the deposition of the PI film. After the deposition of the PI film on the aluminum surface, a very thin semi-transparent gold electrode with thickness of about 200 Å and area of 10 mm^2 was deposited on the PI surface to form the top electrode. The thickness of the PI film used was about 2.5 μm to ensure that the illuminating light through the Au electrode would be completely absorbed by the PI film, no residual light illuminating the opposite aluminum electrode.

A 50 W deuterium lamp was used as the UV light source. The lamp was mounted in a housing with spherical mirror, lens and slit to provide a paralleled beam. The illumination beam was chopped to produce rectangular light pulses. For all experiments the light intensity was kept constant. The photocurrent was measured using a Keithley 610 C electrometer in conjunction with a HP-7132 A strip recorder. Blank test of the sample holder inside the chamber showed a stray current less than

5.0x 10^{-14} A with and without light illumination, which was much smaller than the measured currents. The experimental arrangement is shown in figure 4.1.

All electrical measurements were carried out in a vacuum chamber with pressure below 10^{-3} torr to prevent ions produced by the UV light in the surrounding medium from entering the current collecting electrodes and leads. We also checked the temperature rise due to the UV light, which was negligible.

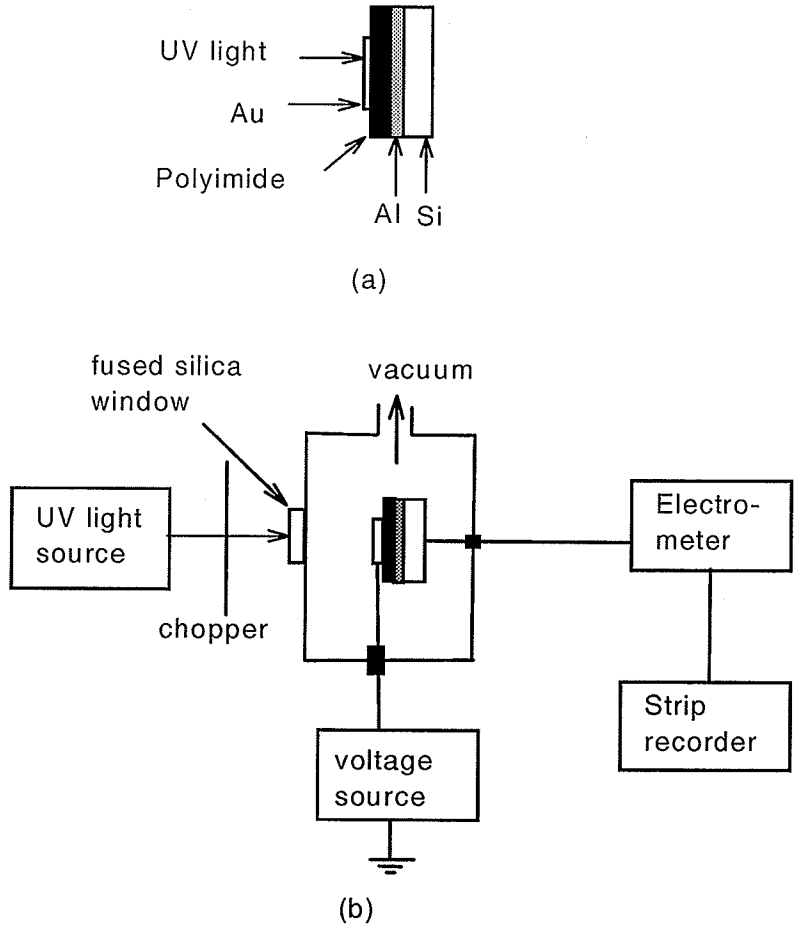

Figure 4.1: *(a) Au-PI-Al structure. (b) Experimental setup for transient photocurrent measurements.*

4.2 Results and Discussion

Figure 4.2 shows the spectrum of the light intensity from Deuterium lamp which has been calibrated[15]. The charging current J_c was measured after the application of a step-function dc voltage and discharging current J_d was measured after the removal of the applied voltage. A series of UV light pulses was switched on to illuminate the sample through the transparent gold electrode. Figure 4.3 and 4.4 show the results under applied voltages of 200 V and 400 V (corresponding to the average electric field 800 kV/cm and 1.6MV/cm). These measurements were taken at the maximum intensity of incident light from the UV lamp (50 W). With the illuminated electrode biased with a positive voltage at a field of 800 KV/cm, the photocurrent rises monotonically until it reaches the steady state value. However, with same polarity on the illuminated electrode but a field of 1.6 MV/cm, the photocurrent immediately reaches its maximum value and then decays gradually with time as shown in figure 4.3 (b). With the illuminated Au electrode is negatively biased at a field of 800 KV/cm , the photocurrent rises abruptly to the peak value and then decays rapidly with time during illumination.

In polyimide there are both acceptor-like and donor-like states which tend to trap electrons and holes, respectively. For the polyimide used for the present investigation, the concentration of acceptor-like states (electron traps) is much higher than that of the donor-like states (hole traps). It has been reported[7] that incorporation of donor-loaded material in polyimide causes an increase by several orders of the photocurrent, indicating the formation of charge-transfer complexes by

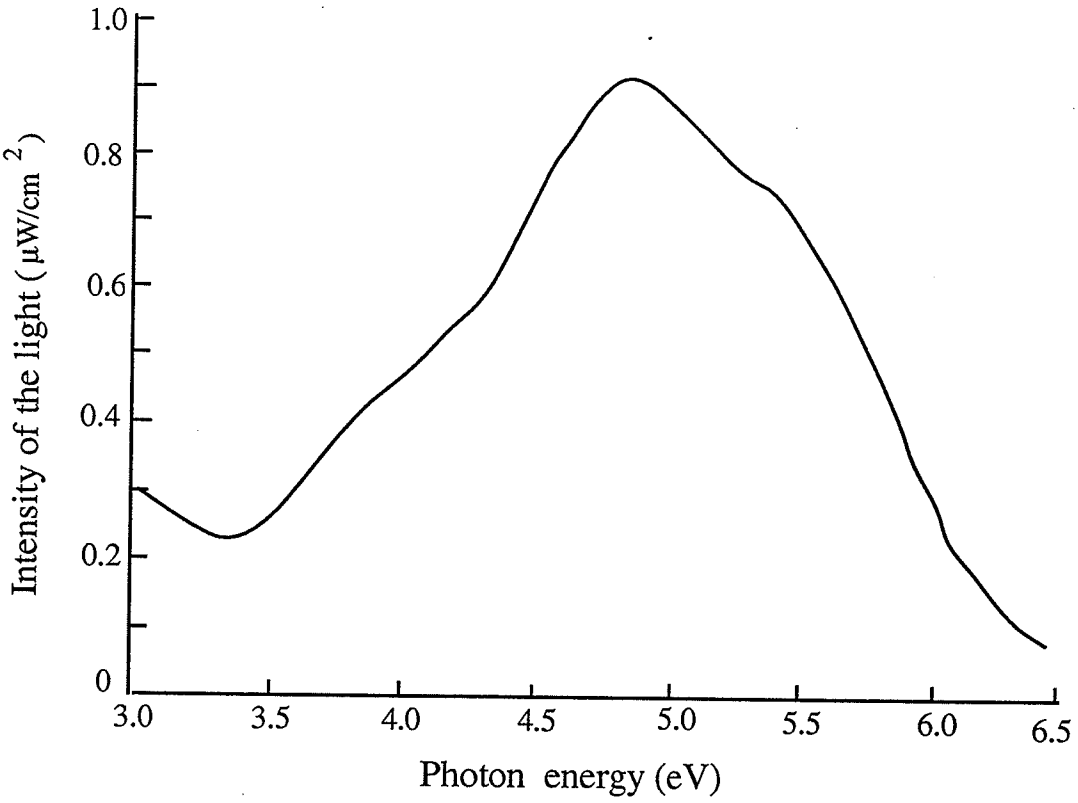

Figure 4.2: *Spectra of the incident light from the Deuterium lamp.*

the existing acceptor-like states coupled with the incorporated donor-like states. We believe that charging current is due to electron trap filling processes. It is likely that at low fields such as 800 KV/cm, the electron injection is due to Schottky-type thermionic emission, while at high fields such as at 1.6 MV/cm, the electron injection is due to Fowler-Nordheim type tunneling process. The energy band gap of polyimide is about 8 eV, the UV illumination (< 6 eV) can only excite an electron from the valence band to an electron trap producing a free holes, or excite an electron from the trap to the conduction band producing a free electron. However, the concentration of electron traps is much larger than the hole traps, therefore the

lifetime of a free hole is much longer than the lifetime of a free electron. This is why the carriers for photoconduction are holes. The lifetime of the free holes depend on the concentration of the trapped electrons (filled traps) which act as hole traps. Tahira and Kao [74] have suggested the following three processes operating simultaneously, and they are, (i) the increase of the filling of the acceptor-like traps by electrons injected from the cathode, so that they become to act as deep hole traps. (ii) the increase of the electron-filled acceptor-like traps by electrons produced by photogeneration and (iii) the holes trapped in the originally existing donor-like traps as well as newly created hole traps.

The injected free and trapped electrons are initially concentrated near electron-injecting contact (cathode) as shown in figure 4.5 partly because the concentration of traps is generally high near the cathode. It would take quite a length of time for them to travel to the opposite contact (anode). Thus during the early stage of the charging period the concentration of trapped electrons is small near the anode. When the light pulses are illuminating the sample through the anode, the pulsed photocurrent increases with time as shown in figure 4.3 (a), Indicating that the hole lifetime is relatively long. In other words, the rate of photogeneration of holes is larger than the rate of holes being trapped during the light pulses. This is for the case of low field of 800 KV/cm. When the applied field is increased to 1.6 MV/cm, the concentration of trapped electrons (hole traps) is large. Under this condition, the rate of photogeneration of holes becomes gradually smaller than the rate of holes being

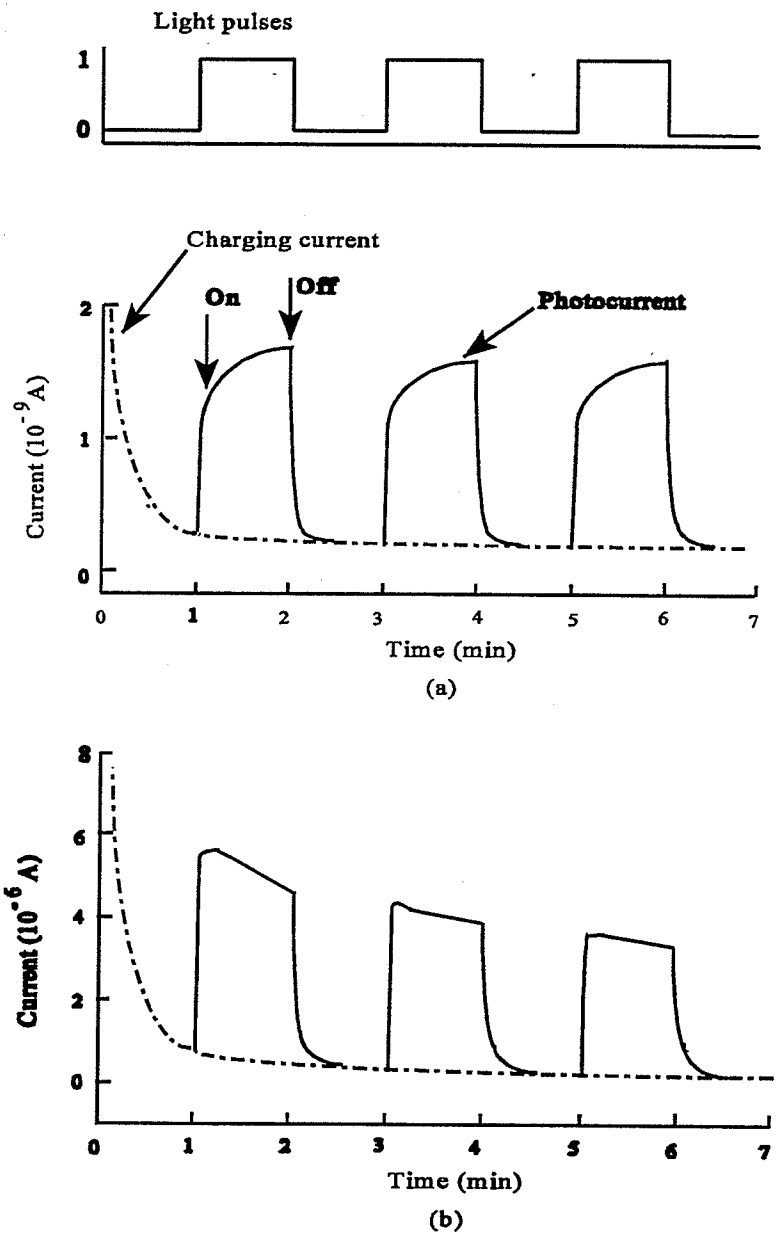

Figure 4.3: *The photocurrent transient superimposed on the charging current with the illuminated electrode positively biased at (a) 800 kV/cm. (b) 1.6 MV/cm.*

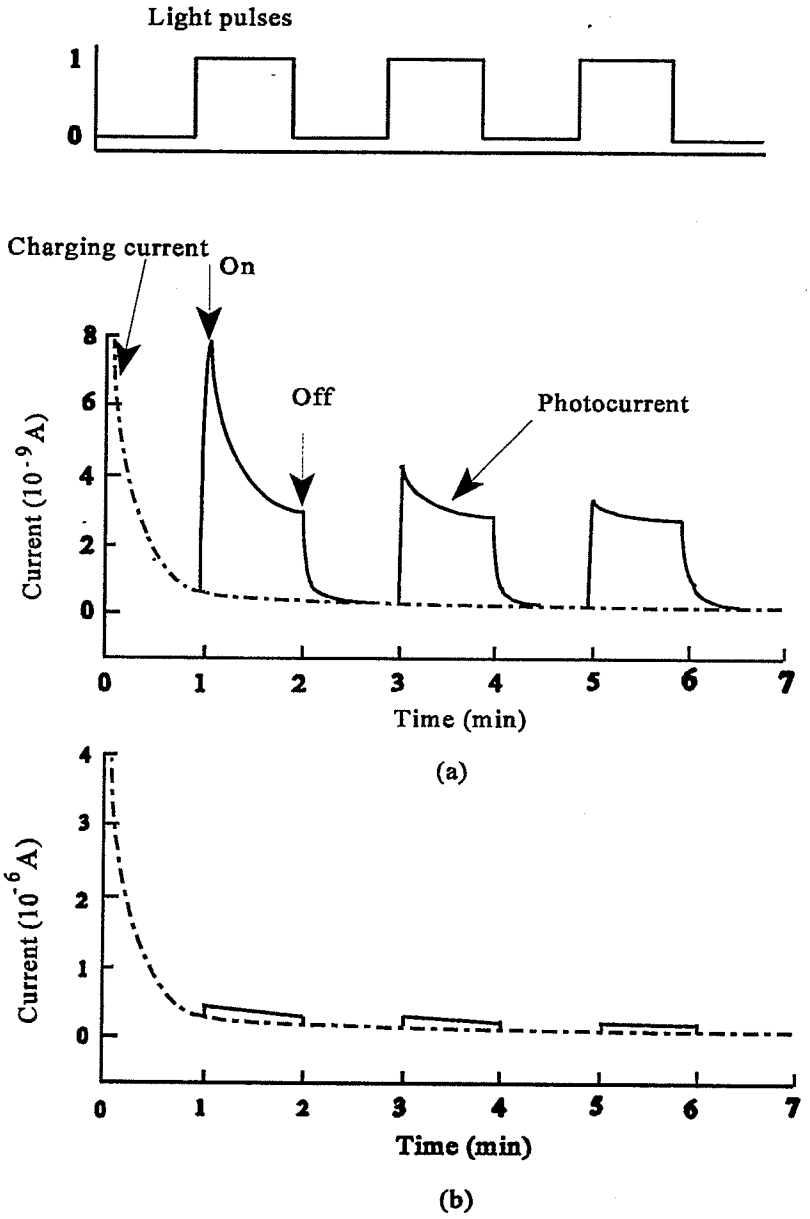

Figure 4.4: *Photocurrent transient superimposed on the charging current with illuminated electrode negatively biased at (a) 800 kV/cm (b) 1.6 MV/cm.*

trapped. This is why the photocurrent decreases with time during the light pulses as shown in figure 4.3 (b).

When the light pulses are illuminating the sample through the negative illuminated electrode (cathode), the photocurrent decays very rapidly with time as shown in figure 4.4(a) for the field of 800 KV/cm. This is attributed to the fact that in the early stage of the charging period the concentration of injected trapped electrons near the cathode is very large as compared with these near the anode as shown in figure 4.5. So the lifetime of the photogenerated minority holes is small, and the rate of photogeneration of holes becomes less than the rate of holes being trapped. As the applied field is increased to 1.6 MV/cm, a large quantity of electrons will be injected by FN type of tunneling. The rate of annihilation of photogenerated holes becomes so large, the photocurrent is very small as shown in figure 4.4 (b).

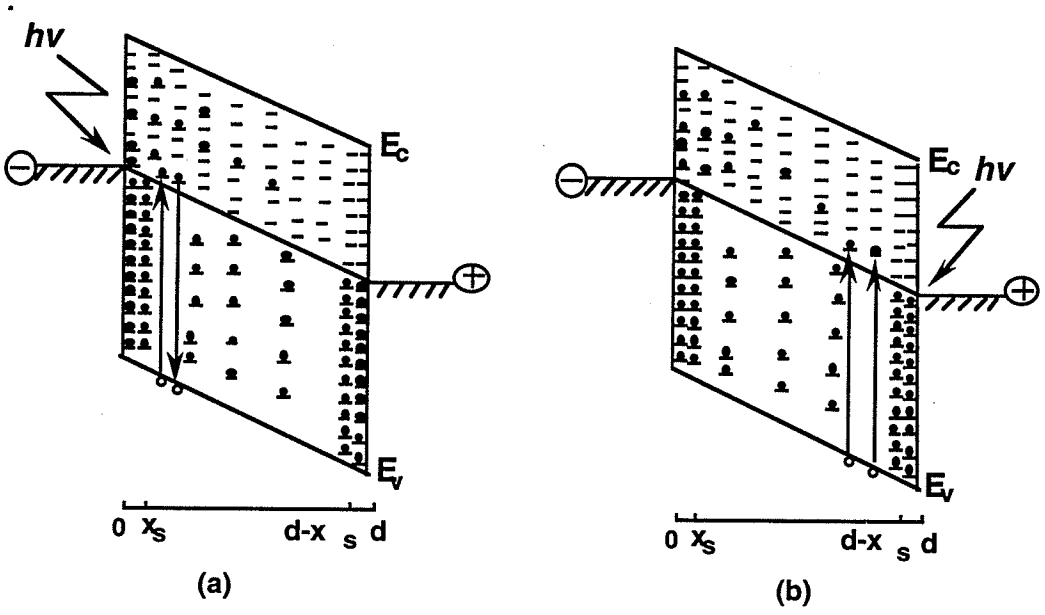

Figure 4.5: *The photogeneration processes during the charging period: (a) for light illuminating the negatively biased electrode (short hole life time), and (b) for light illuminating the positively biased electrode (long hole life time) (after Tahira and Kao [74]).*

After the charging current has almost reached it minimum steady state value, short-circuiting the two electrodes will result in a discharging current which is mainly produced by the thermal detrapping of the trapped electrons and then the discharging of the electrons at both electrodes. At the time of short-circuiting, the concentration of trapped carriers is higher near the carrier-injecting electrode and decreases with increasing distance from the injecting contact. There exists a point x* at which the internal field F = 0 as shown in figure 4.6. As the time goes on, the point x* tends to move toward the center of the sample at which x= d/2. During this movement, there is a net discharging current flow in the external circuit with the photocurrent flow in the same direction as that of the discharging current as shown in figure 4.7 (a) and (b) and figure 4.8 (a) and (b). The net dark discharging current can be written as ,

$$J_d = | J_{t1} - J_{t2} | = q n_t(x^*)(dx^*/dt)$$

where J_{t1} and J_{t2} are currents flowing out of two electrodes as shown in figure 4.6, $n_t(x)$ is the concentration of trapped electrons at x*.

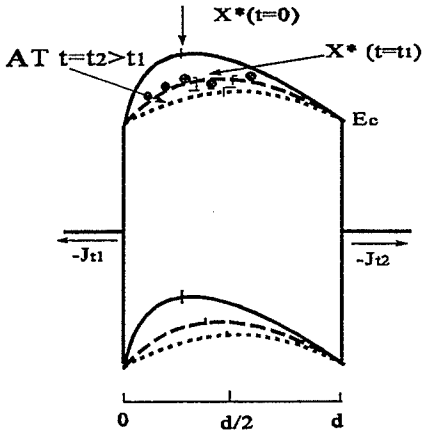

Figure 4.6 *Illustrating the dark electron current j_{t1} and j_{t2} flowing out of two electrodes during the discharging period with negatively biased at x=0 during the charging period.*

At relatively low field (800 KV/cm), the electron injection may be mainly due to Schottky type thermionic emission. The concentration of electron-filled traps is always higher near the electron injecting contact. As the barrier height for electron injection is always smaller than that for hole injection from metal to polyimide, we can assume that the hole injection is much smaller than the electron injection. Thus for the illuminated electrode at the positive polarity, the photogenerated electrons will be trapped by the traps, leaving free holes. So the carriers responsible for photoconduction are mainly holes. Obviously, the photocurrent would decreases with time, partly due to the decrease of the internal field as the x* moves toward the center of PI. When the illuminated electrode is at negative polarity, the photocurrent is much smaller than that at positive polarity as shown in figure 4.7. This is due to higher concentration of trapped electrons available near the cathode to capture the photogenerated holes resulting a lower photocurrent.

During the discharging process at relatively high field (1.6 MV/cm), the basic concept is the same with the photoconduction process at low field (800 KV/cm), that is, the annihilation of the photogenerated hole carriers by trapped electrons. However, we should note that electron injection from the injecting contact is due to the Fowler-Nordheim type injection rather than Schottky type thermionic injection (during the charging process). The results are shown in figure 4.8.

As has been already mentioned, most photocurrent measurements in the past were after the charging current had reached its quasi-steady-state dc value. This

marks the role played by the electron-filled traps in the electrical transport processes, and this is also why some investigators did not find the dependence of the photocurrent on the dark charging current[73]. Our results show that the that the photocurrent depends strongly on the magnitude of the charging and the discharging currents. This dependence indicates clear that the deep holes traps created by the filling of the acceptor-like electron traps injected electrons play a more important role than the originally existing donor-like hole traps in the photoconduction processes.

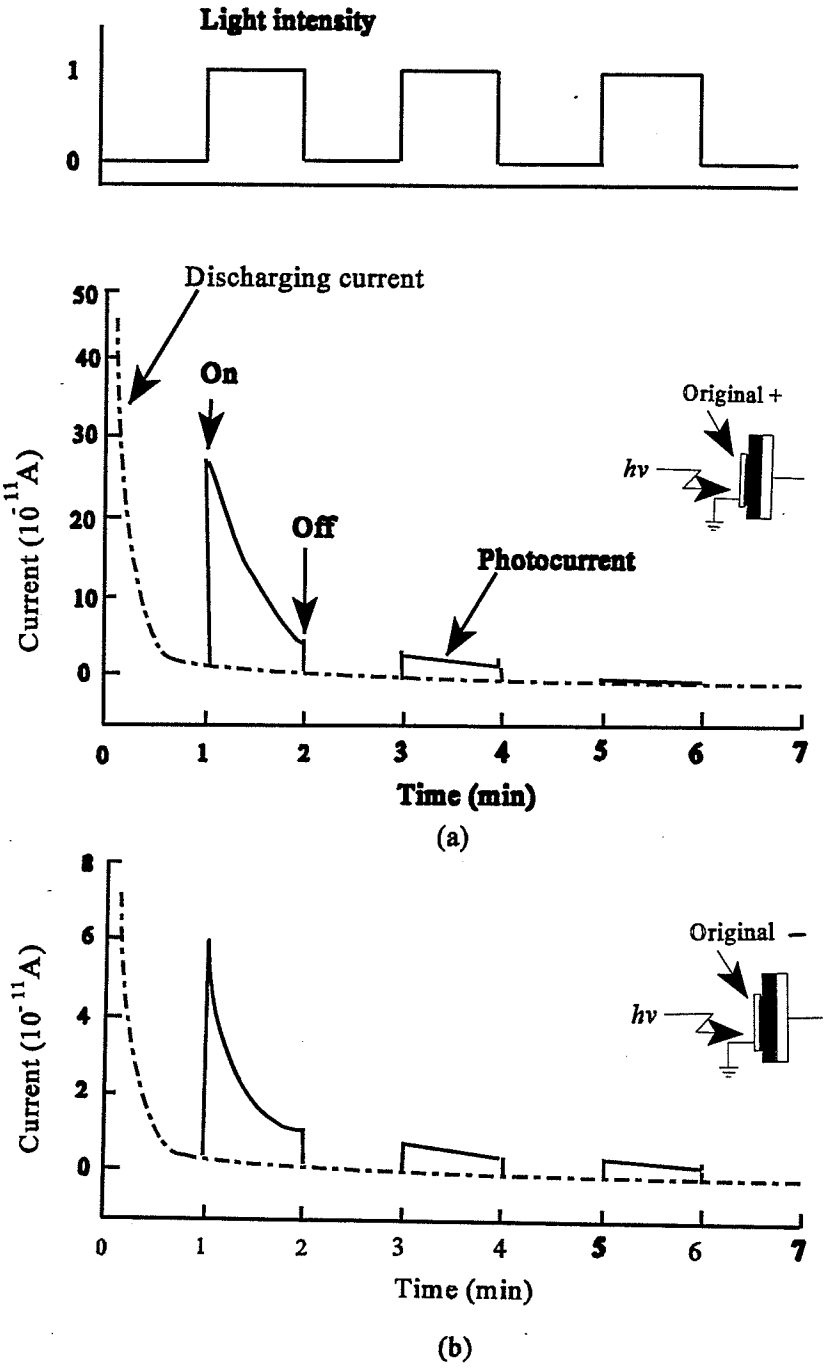

Figure 4.7 *The photocurrent superimposed on the discharging current (a) the illuminated electrode positively biased at 800 KV/cm (b) the illuminated electrode negatively biased at 800 KV/cm.*

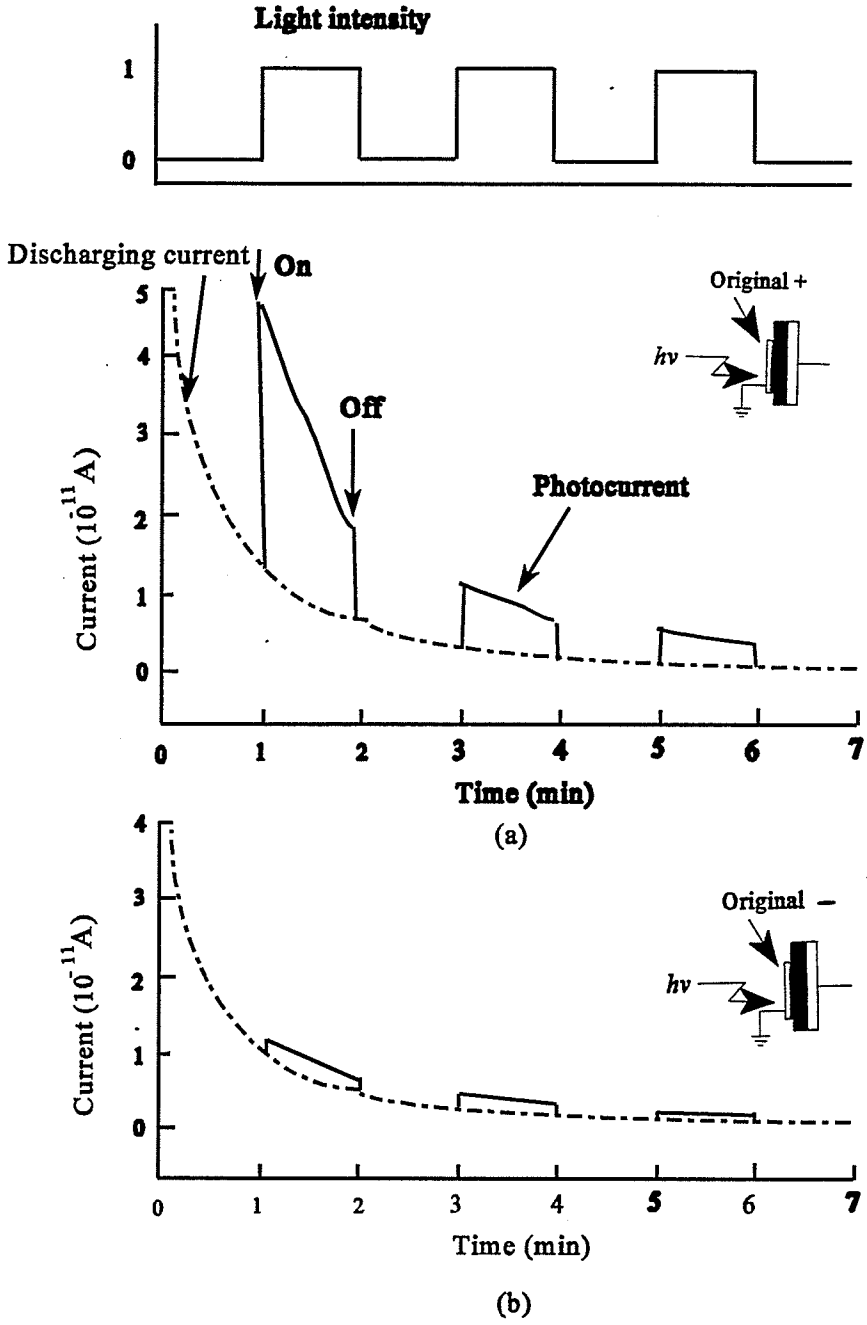

Figure 4.8 *The photocurrent superimposed on the discharging current (a) the illuminated electrode positively biased at 1.6 MV/cm. (b) the illuminated electrode negatively biased at 1.6 MV/cm.*

Chapter 5

Conclusions

On the basis of the experimental results discussed above, the following conclusions are drawn.

(1) At electric fields below the threshold field, either a positive or a negative trapped charge is formed, which is dependent on the polarity of the applied gate voltage. This charge produces the hysteresis of the C-V loop.

(2) The threshold field for the onset of the Fowler-Nordheim type of electron tunneling is about 1.4 MV/cm and the electrons are dominant carriers at high electric fields.

(3) The conduction current and the average breakdown strength are strongly dependent on the humidity. Electric breakdown is initiated by the thermal instability and then followed by the creation of large mean free paths for the subsequent impact ionization leading to a sharp rise of the current.

(4) Due to a large density of deeply trapped electrons near the interface between the PI and Si, a ledge always occurs when the gate is positively biased and

computer simulation shows that for the ledge to occur, the effective sheet trap density ranging from 10^{12} to 10^{13} cm^{-2} .

(5) The dark charging and discharging currents are mainly due to the trapping and the thermally activated detrapping processes.

(6) The photocurrent decay during charging and discharging period is due to the decrease of the lifetime of the photogenerated holes by the increase of the electron-filled acceptor like traps.

(7) The photocurrent transients are dependent on the applied electric field and the polarity of the illuminated electrode. Photogenerated free carriers under UV light in polyimide are mainly holes. The lifetime of these holes are strongly dependent on the presence of the trapped electrons.

References

[1] Sugimoto, E., *IEEE Electrical Insulation Magzine*, 5, No.1 (1989)

[2] Rothman, L. B., *J. Electronchem. Soc.* October (1980)

[3] Sacher, E., *IEEE Trans. Elec. Insul.* EI-14, pp. 85, (1979).

[4] Sanchez, D., Carchano, M. and Bui, A., *J. Appl. Phys.* 45, pp. 1233, (1974).

[5] Barlett, R. H., Fulk, G. A., Lee, R. S., and Weingart, W., *IEEE Tran. Nucl. Sci.*, NS-22, pp. 2273, (1979).

[6] Weingart, R. C., Bartlett, R. H., Lee, R. S., and Hofer, W., *IEEE Trans. Nucl. Sci.* NS-19, pp. 15, (1979).

[7] Freilich, S. C., *Macromolecules*, 20, pp.973, (1987).

[8] Lafemina, J. P., Arjavalingam, G., and Hougham, G., *J. Chem. Phys.* 90, pp. 5154, (1989).

[9] Serafini, T. T., *High temperature resins.* In handbook of composites, (Ed. Lubin, G.), New York, (1982).

[10] Kreutz, J. A., Endery, A. L., Gray, F. P., Sroog, C. E., *J. Polymer Sci.*, Part A-14, pp.2607 (1966).

[11] Dine-Hart, R. A., Wright, W. W., *Die Makromolekulare Chemie*, 143, pp. 189, (1971).

[12] Ginsburg, R., Susko, J. R., in "*Polyimides*", (Ed. , Mittal, K. L.,) Plenum Press, New York, pp. 237, (1982).

[13] Denisov, V. M., Koltsov, A. L., Mikhailova, N. V., Nikitin, V. N., Bessonov, M. I., Glukhov, N. A., Shcherbakova, *Polymer Sci. USSR*, 18, pp.1780, (1976).

[14] Krasovskii, A. N., Antonov, N. P., Koton, M. M., Kainin'sh, K. K., Kudryavtees, V. V., *Polymer Sci. USSR* 21, pp.1038, (1980).

[15] Kan, L., and Kao, K. C., *J. Chem. Phys.*, 98, pp. 3345, (1993).

[16] Johnsin, C., Mao, J., and Wunder, S. L., In "*Polyimides: Materials, Chemistry and Characterization.*" (Ed. Feger, C. *et al*) Elsevier Science Publishers B. V., Amsterdam, (1989).

[17] Russell, T. P., Gugger, H., and Swalen, J. D., *J. Polymer Sci. Polym. Phys.* Ed. 21, (1983).

[18] Takahashi, N., Yoon, D. Y., and Parrish, W., *Macromolecules,* 17, pp. 2583, (1984).

[19] Isoda, S., Shimada, H., Kochi, M., and Kambe, H., *J. Polym. Sci. Polym. Phys.* Ed. 19, pp.1293, (1981).

[20] Wellingholf, S. T., Ishida, H., Koeing, J. L., and Baer, E., *Macromolecules,* 13, (1980).

[21] Hergenrother, P. M., wakelyn, N. T., and Havens, S. T., *J. Polym. Sci. Part A: Polym. Chem.*, 25, pp.1093, (1987).

[22] Critchley, J. P., Grattan, P. A., White, M. A., and Pippett, J. S., *J. Polym. Sci.*, A-1, 10, pp.789, (1972).

[23] Hougham, G., Tesoro, G., and Shaw, J., In *"Polyimides: Materials, Chemistry and Characterization."* (Ed. Feger, C. *et al*) Elsevier Science Publishers B. V., Amsterdam, (1989).

[24] Hanscomb, J. R., and Calderwood, J. H., *J. Phys. D: Appl. Phys.*, 13, pp.1093, (1973).

[25] Harada, Y., Matsumoto, F., and Nakado, T., *This Journal*, 130, pp.129, (1983).

[26] *Polymer Materials for Electronic Applications*, edited by Feit, E. D. and Wilkins, C. W., American Chemical Society, (1982).

[27] Nagao, M., Kitamura, T., Mizuno, Y., Kosaki, M., and Ieda, M., Proc. *3rd int. Conf. on Conduction and Breakdown in Solid Dielectrics*, Trondheim, Norway, pp.77, (1989)

[28] Nevin, J. H., and Sunme, G. L., *Microelectronics and Reliability*, 21, pp.669, (1981).

[29] Sessler, G. M., Hahn, B., and Yoon, D. Y., *J. Appl. Phys.*, 60, pp.318, (1986).

[30] Sacher, E. *IEEE Tran. Elec. Insul.*, 13, pp.1093, (1973)

[31] Sawa, G., Nakamura, S., Iida, K., and Ieda, M., *Jan. J. Appl. Phys.* 19, pp. 453, (1980).

[32] Sharama, B. L., and Pillai, *PKC, Physica Status Solidi., 34, (1982).*

[33] Smith, F. W., Neuhaus, H. J., Senturia, S. D., Feit, Z., Day, D. R., and Lewis, T.J., *J. Electronic materials*, 16, pp.93, (1987).

[34] Lewis, T. J., *IEEE Trans. Elect. Insul.* 19, pp.210, (1984).

[35] Neuhaus, H. J., Hershkowitz, G. B., and Senturia, In *"Polyimides: Materials, Chemistry and Characterization."* (Ed. Feger, C. *et al*) Elsevier Science Publishers B. V., Amsterdam, (1989).

[36] Hikita, M., Hirose, T., Ito, Y, Mizutani, T., and Ieda, M., *J. Phys. D.*, 23, pp.1515, (1990).

[37] Takai, Y., Kim, M. M., Kurachi, A., Mizutani, T., and Ieda, M., *Jan. J. Appl. Phys.*, 21, 1524, (1982).

[38] Denton, D. D., Buncick, M. C., and Pranjoto, H., *J. Mat. Res.*, 6, pp.2747, (1991).

[39] Buncick, M. C., and Denton, D. D., *J. Appl. Polym. Sci.*, pp.1254, (1992).

[40] Xu, G., Gryte, C. C., Nowick, A. S., Li, S. Z., Pak, Y. S., and Greenbaum, S.G., *J. Appl. Phys.* 66, pp.5290, (1989).

[41] Melcher, J., Yang, D., and Arlt, G., *IEEE Trans. Elec. Insul.* 24, pp.31, (1989).

[42] Vchimura, S and Makino, D., In *"Polyimides: Materials, Chemistry and Characterization."* (Ed. Feger, C. *et al*) Elsevier Science Publishers B. V., Amsterdam, (1989).

[43] Gonsalves, K., Parekh, P., Hollawd, R., Bocarsly, A., Arbucklo, G., In *"Polyimides: Materials, Chemistry and Characterization."* (Ed. Feger, C. *et al*) Elsevier Science Publishers B. V., Amsterdam, (1989).

[44] Senturia, S. D., Presented at the Polyimide Symposium, California, September, (1986).

[45] Nelson, T. T., *et al* , Bell Telephone Laboratories, IEEE , pp.244, (1980).

[46] Cook, H. C., Farrar, P. A., Vttecht, R. R., and Wilson, J. P., *IBM Techn. Disc. Bull.* ,16, pp. 728, (1983).

[47] Sato, K., *et al, IEEE Trans. on Parts, Hybrids, and Packaging*. PHP-9, pp.176, (1973).

[48] Shen, W. H., Yo, A. J., and Gong, B. M., *Polyimides. synthesis, Characterization, and Applications,* Vol. 2, Mittal, K. L., ed., Plenum Press, pp947, (1984).

[49] Rubner, R., *"Polyimide Film Patterns."* Siemens Forsch.-u. Entwickl.-*Ber.* 5, 235, (1976).

[50] Schubert, P. J., and Nevin, J. H., *IEEE Trans. Electron Devices*, ED-32, pp.1220, (1985).

[51] Denton, D., Ho, C. C., and He, S., *IEEE Tran. Instrumentation and Measurement* 39, No. 3, pp.508, (1990).

[52] Hahn, B. R. and Yoon, D. Y., *J. Appl. Phys.* 65, pp. 2766, (1989).

[53] Ning, T. H., and Yu, H. N., *J. Appl. Phys.* 45, pp.5373, (1974).

[54] Chen, C. , and Wu, C., Solid state electronics, 29, pp.1059, (1986)

[55] Kao, K. C., *J. Appl. Phys.* 55, pp.752, (1984).

[56] Mizutani, T., Kanno, I., Hikita, M., and Ieda, M., *IEEE Tran. Elec. Insul.* 22, pp. 473, (1987)

[57] Xie, H. K., and Kao, K. C., *IEEE Tran. Elec. Insul.* 17, pp.221, (1982).

[58] Sze, M. S., *Physics of semiconductor devices,* McGraw-Hill, New York, (1985).

[59] Kern, W., and Puotiue, D. A., *RCA Rev.* 31, pp.187, (1970).

[60] Chau, T. T., Mejia, S. R., and Kao, K. C., *J. Vac. Technol.* B9(1), pp.50, (1991).

[61] Liu, D., and Kao, K. C., *J. Appl. Phys.* 69, pp.2489, (1991).

[62] Davies, D. K., and Look, P. J., *J Electrochem. Soc. Sol. State Sci. Tech.* 120, pp.216, (1973).

[63] Davies, D. K., *IEEE Proc.* Vol. 128, pp.153, (1981).

[64] Duck, C. B., and Fabish, T. J., *J. Appl. Phys.* 49, pp.315, (1978).

[65] Murata, Y., Jan. *J. Appl. Phys.* 18, pp.1, (1979).

[66] Lenzlinger, M., and Snow, E. H., *J. Appl. Phys.* 40, pp.278, (1969).

[67] Pulfrey, D. L., Shousha, A. H. M. and Young, H., *J. Appl. Phys.* 41, pp.2838, (1970).

[68] Kowalczyk, S. P., *Phys. Rev. B* 41(3), pp.1645, (1990)

[69] Caranahan, B., Luther, H. A., and Wilkes, J. O., *Applied Numerical Methods,* pp. 361, Wiley, New York, (1969).

[70] Miyairi, K., Jan. *J. Appl. Phys.* 33, pp.1397, (1994).

[71] Wintle, H. J., *IEEE Trans. Electr. Insul.* EI-12, 97, pp.424, (1977).

[72] Wintle, H. J., and Tibensky, G. M., *J. Polym. Sci.* 11, pp.25, (1973).

[73] Garton, C. G., *J. Phys. D, Appl. Phys.*, 7, pp.1814, (1974).

[74] Tahira, K., and Kao, K. C., *J. Phys. D, Appl. Phys.* 18, pp.2247, (1985).

Appendix

Computer program for simulation of I-V characteristics

ntu@mira.cc.umanitoba.ca ccp Tue Jul 11 14:18:38 1995

(stdin)

In the following program, using maple software

$a_1 = q[F_c(t)]^2 m/(16\pi^2 \hbar m^*)$; $a_2 = 4(2m^*)^{1.5}/3h$; $a_3 = q/\varepsilon_{PI}$; $a_4 = q^3/(4\pi\varepsilon_{PI})$ epsai=σ; faibo=ϕ_{PI}.

The computer program for the simulation results in figure 3.11.

```
proc()
  k := 0;
  gh := array(0 .. 10);
  for Nt from 20000000000000000 by
    10000000000000000 to
    50000000000000000 do
    a1 := .7820000000*10^(-25);
    a2 := .1200000000*10^38;
    a3 := .5320000000*10^(-8);
    a4 := .4230000000*10^(-9);
    q := .1600000000*10^(-18);
    epsai := 1/10000000000000000000;
    faibo := 3.8 ;
    g := 1.7 ;
    d := .6500000000*10^(-6);
    faims := 0;
    A := .1770000000*10^(-5);
    Xc := 0;
    de1 := {subs(j = a1*Fc^2*
      exp(-a2*faib^1.5*q^1.5/Fc)/faib
      /q,faib = faibo-a4^.5*Fc^.5,Ec
       = (g*t-faims+.1*10^(-1))/d-
      n(t)*a3*(1-Xc),
      D(n)(t) = epsai*j*(Nt-n(t))/q),
      n(0) = 0};
    F := dsolve(de1,n(t),numeric);
    with(plots);
    re1 := subs(w =
      (g*t-faims+.1 )/d-n(t)*a3*(1-Xc)
      ,w);
    re2 := subs(re1 = re1,
      faib = faibo-a3^.5*re1^.5,
      .1190000000*10^(-9)+A*a1*re1^2*
      exp(-a2*faib^1.5*q^1.5/re1)/
      faib/q);
    k := k+1;
    gh[k] :=
      odeplot(F,[t,re2],0 .. 180)
  od;
  logplot({gh[1],gh[2],gh[3],gh[4]})
end
```

The computer program for the simulation results in figure 3.12.

```
proc()
  k := 0;
  gh := array(0 .. 10);
  for Xc from 0 by .5  to 1 do
    Nt := 40000000000000000;
    a1 := .7820000000*10^(-25);
    a2 := .1200000000*10^38;
    a3 := .5320000000*10^(-8);
    a4 := .4230000000*10^(-9);
    q := .1600000000*10^(-18);
    epsai := 1/10000000000000000000;
    faibo := 3.8 ;
    g := 1.7 ;
    d := .6500000000*10^(-6);
    A := .1770000000*10^(-5);
    faims := 0;
    de1 := {subs(j = a1*Fc^2*
      exp(-a2*faib^1.5*q^1.5/Fc)/faib/
      q,faib = faibo-a4^.5*Fc^.5,Fc =
      (g*t-faims+.1 )/d-n(t)*a3*(1-Xc)
      ,D(n)(t) = epsai*j*(Nt-n(t))/q),
      n(0) = 0};
    F := dsolve(de1,n(t2),numeric);
    with(plots);
    re1 := subs(w =
      (g*t-faims+.1 )/d-n(t)*a3*(1-Xc)
      ,w);
    re2 := subs(re1 = re1,
       faib = faibo-a4^.5*re1^.5,
       .1190000000*10^(-9)+A*a1*re1^2*
       exp(-a2*faib^1.5*q^1.5/re1)/
       faib/q);
    k := k+1;
    gh[k] :=
       odeplot(F,[t2,re2],0 .. 180)
  od;
  logplot(
    {gh[1],gh[2],gh[3]},xtickmarks = 5)
end
```